# Mechanisms underlying an impairment of visual response properties in mouse models of Alzheimer's disease

**Dissertation**

**zur Erlangung des Grades eines**
**Doktors der Naturwissenschaften**

**der Mathematisch-Naturwissenschaftlichen Fakultät**
**und**
**der Medizinischen Fakultät**
**der Eberhard Karls Universität Tübingen**

**vorgelegt**
**von**

**Nithi Asavapanumas**
**aus Bangkok, Thailand**

**Dezember 2018**

Tag der mündlichen Prüfung: 26 April 2019

Dekan der Math.-Nat. Fakultät: Prof. Dr. W. Rosenstiel
Dekan der Medizinischen Fakultät: Prof. Dr. I. B. Autenrieth

1. Berichterstatter: Prof. Dr. Olga Garaschuk

2. Berichterstatter: Prof. Dr. Laura Busse

- Prüfungskommission: Prof. Dr. rer. nat. Thomas Euler
  Prof. Dr. Olga Garaschuk
  Prof. Dr. Laura Busse
  Prof. Dr. Manuela Neumann

# Abstract

Alzheimer's disease (AD) is a progressive neurodegenerative disorder, which affects around 50 million people worldwide. Besides impairment of memory and cognition, which are common in AD, it is accompanied by an impairment of visual processing. Up to now there is no curative therapy for AD. The available drugs provide only symptomatic treatment, which has no effect on the causes of the disease. Therefore, a better understanding of the underlying causes and the identification of new therapeutic targets are required.

Recently, neuronal hyperactivity has been widely recognized as one of the key functional impairments in AD as well as in the normal ageing. Previous study suggested the relationship between neuronal hyperactivity and the visual impairments in the mouse model of AD. However, the underlying mechanisms remain unclear. Using *in vivo* two photon $Ca^{2+}$ imaging, the effect of ageing, an obvious risk factor of AD, on the ongoing neuronal activity in the primary visual cortex (V1) of 3, 10-12 and 18 months old mice were first characterized in this study. Ageing-related neuronal hyperactivity was found in 18 months old mice and was accompanied by an impairment of orientation tuning without changes in the direction tuning and visual responsiveness. Interestingly, the age-dependency of ageing-related neuronal hyperactivity in V1 is differs from that found in the frontal/motor cortex, suggesting a differential regional vulnerability to ageing.

Subsequently, animal models of AD were used to study AD-related changes in neuronal properties in V1. We found neuronal hyperactivity in V1 of $APP_{SWE}/PS1_{G384A}$ and $PS1_{G384A}$ mice, which lack amyloid plaque deposition and neuroinflammation. AD-related neuronal hyperactivity in V1 was accompanied by an over-responsiveness to visual stimuli and impaired visual tuning properties (both direction and orientation selectivity) of individual neurons. These impairments were largely caused by an insufficient suppression of responses to non-preferred orientation/direction stimuli. Moreover, visual stimulation robustly suppressed the ongoing spontaneous activity in WT but not in $APP_{SWE}/PS1_{G384A}$ mice.

Finally, we tested the effect of reducing store-mediated neuronal hyperactivity on the impairment of visual processing in AD mice. Emptying intracellular $Ca^{2+}$ stores significantly reduced neuronal hyperactivity and the pathological over-responsiveness to visual stimuli but could not rescue stimulus-induced suppression of spontaneous activity and impaired tuning properties of individual cells. Thus, our data identify the AD-mediated dysfunction of intracellular $Ca^{2+}$ stores as a main cause of pathologically increased visual responsiveness in $APP_{SWE}/PS1_{G384A}$ mice. However, the impairment of visual tuning and the stimulus-induced suppression of spontaneous activity, identified in this study, are likely caused by different mechanisms, for example, dysfunction of local interneurons.

# Zusammenfassung

Die Alzheimer-Krankheit (AD) ist eine neurodegenerative Erkrankung, von der weltweit rund 50 Millionen Menschen betroffen sind. Neben den üblichen Beeinträchtigungen des Gedächtnisses und der Kognition ist auch die visuelle Verarbeitung im Rahmen der AD verändert. Bislang gibt es keine kurative Therapie für die Erkrankung. Die verfügbaren Medikamente bieten lediglich eine symptomatische Behandlung, die keinen Einfluss auf die Ursachen der Krankheit hat. Daher ist ein besseres Verständnis der zugrunde liegenden Ursachen und die Identifizierung neuer therapeutischer Einsätze erforderlich.

Die neuronale Hyperaktivität ist mittlerweile sowohl bei AD als auch bei der normalen Alterung als eine der wichtigen funktionellen Beeinträchtigungen allgemein anerkannt. Bereits aus früheren Studien geht ein Zusammenhang zwischen neuronaler Hyperaktivität und visueller Beeinträchtigung im Mausmodell der Erkrankung hervor. Die zugrunde liegenden Mechanismen sind jedoch unklar. Altern stellt einen offensichtlichen Risikofaktor für AD dar. Diese Studie charakterisiert mit Hilfe von *in vivo* Zwei-Photonen-Mikroskopie und $Ca^{2+}$-Bildgebung erstmals die Auswirkungen des Alterns auf die neuronale Aktivität im primären visuellen Kortex (V1) von 3, 10-12 und 18 Monate alten Mäusen. Altersbedingte neuronale Hyperaktivität wurde bei 18 Monate alten Mäusen festgestellt. Diese wurde von einer Beeinträchtigung des Orientierungstunings, jedoch nicht des Richtungstunings oder der visuellen Reaktionsfähigkeit der Neurone, begleitet. Interessanterweise unterscheidet sich die Altersabhängigkeit der neuronalen Hyperaktivität in V1 von derjenigen im frontalen/motorischen Kortex, was auf eine unterschiedliche regionale Anfälligkeit für das Altern hindeutet.

Weiterhin wurden Tiermodelle der Alzheimer-Krankheit verwendet, um den Einfluss der Erkrankung auf die neuronalen Eigenschaften in V1 zu untersuchen. Wir fanden neuronale Hyperaktivität in V1 von $APP_{SWE}/PS1_{G384A}$ und $PS1_{G384A}$ Mäusen. Letztere haben keine Amyloidablagerungen und weisen keine Anzeichen von Neuroinflammation auf. Die AD-bedingte neuronale Hyperaktivität in V1 wurde von einer

Überempfindlichkeit auf visuelle Reize und einer Beeinträchtigung der visuellen Tuningeigenschaften (sowohl Richtungs- als auch Orientierungsselektivität) einzelner Neuronen begleitet. Diese Beeinträchtigungen wurden vornehmlich durch eine unzureichende Unterdrückung der neuronalen Reaktionen auf nicht-bevorzugte Orientierungs-/Richtungsreize verursacht. Darüber hinaus unterdrückte die visuelle Stimulation die anhaltende spontane Aktivität bei WT-Tieren, nicht aber bei $APP_{SWE}/PS1_{G384A}$-Mäusen.

Zusätzlich haben wir untersucht, welchen Einfluss die $Ca^{2+}$-Speicher-vermittelte neuronale Hyperaktivität auf die visuelle Verarbeitung im Mausmodell der Erkrankung hat. Die Entleerung von intrazellulären $Ca^{2+}$-Speichern resultierte in einer signifikanten Erniedrigung der neuronalen Hyperaktivität und einer Verringerung der pathologischen Überempfindlichkeit auf visuelle Reize. Die Stimulus-induzierte Unterdrückung der neuronalen Spontanaktivität hingegen und die beeinträchtigten Tuning-Eigenschaften einzelner Zellen konnten hierdurch jedoch nicht verbessert werden.

Folglich geht aus unseren Daten hervor, dass die AD-vermittelte Dysfunktion intrazellulärer $Ca^{2+}$-Speicher eine Hauptursache für die pathologisch erhöhte visuelle Überempfindlichkeit bei $APP_{SWE}/PS1_{G384A}$-Mäusen ist. Ursächlich für die in dieser Studie beschriebenen Beeinträchtigungen des visuellen Tunings und der Stimulus-induzierten Unterdrückung der Spontanaktivität sind jedoch wahrscheinlich andere Mechanismen wie z. B. eine Dysfunktion lokaler Interneurone.

# Statement of contributions

This dissertation study was carried out in the Institute of Physiology, Department of Neurophysiology, at the Eberhard Karls Universität Tübingen under the supervision of Professor Dr. Olga Garaschuk. This work was conceived by Professor Dr. Olga Garaschuk.

Experiments that involved $Ca^{2+}$-imaging mentioned in the introduction and the materials and methods section were performed by Dr. Chommanad Lerdkrai. The correlation analysis was performed by Prof. Dr. Peter Martus. I did the experiments and data analysis in this dissertation work by myself.

I wrote this dissertation and a published manuscript entitled "Role of intracellular $Ca^{2+}$ stores for an impairment of visual processing in a mouse model of Alzheimer's disease." under the supervision of Professor Dr. Olga Garaschuk.

The results presented in this study were published in

**Asavapanumas N**, Brawek B, Martus P, Garaschuk O. Role of intracellular $Ca^{2+}$ stores for an impairment of visual processing in a mouse model of Alzheimer's disease. Neurobiol Dis. 2018 Oct 24; 121:315-326. doi: 10.1016/j.nbd.2018.10.015.

Lerdkrai C, **Asavapanumas N**, Brawek B, Kovalchuk Y, Mojtahedi N, Olmedillas Del Moral M, Garaschuk O. Intracellular $Ca^{2+}$ stores control *in vivo* neuronal hyperactivity in a mouse model of Alzheimer's disease. Proc Natl Acad Sci U S A. 2018 Feb 6; 115(6): E1279-E1288. doi: 10.1073/pnas.

# Table of contents

# List of abbreviations

| | |
|---|---|
| AD | Alzheimer's disease |
| aMCI | amnestic mild cognitive impairment |
| ANOVA | analysis of variance |
| ApoE | apolipoprotein E |
| APP | amyloid precursor protein |
| AUC | area under the curve |
| Aβ | amyloid-β |
| $Ca^{2+}$ | Calcium |
| $[Ca^{2+}]_I$ | intracellular calcium concentration |
| CPA | cyclopiazonic acid |
| CR1 | complement receptor type 1 |
| DMSO | dimethyl sulfoxide |
| DSI | direction selectivity index |
| ER | endoplasmic reticulum |
| FAD | Familial Alzheimer's disease |
| fMRI | functional magnetic resonance imaging |
| GEE | Generalized Estimating Equations |
| $IP_3$ | inositol triphosphate |
| $IP_3R$ | inositol triphosphate receptors |
| NA | numerical aperture |

| | |
|---|---|
| NMDA | N-methyl-D-aspartic acid |
| NMDAR | N-methyl-D-aspartic acid receptor |
| OSI | orientation selectivity index |
| PLC | phospholipase C |
| PS1 | presenilin 1 |
| PS2 | presenilin 2 |
| $PV^{+}$ | Parvalbumin positive |
| rANOVA | repeated measures analysis of variance |
| ROIs | regions of interest |
| RyRs | ryanodine receptors |
| SD | standard deviation |
| SERCA | sarco/endoplasmic reticulum $Ca^{2+}$-ATPases |
| TREM2 | triggering receptor expressed on myeloid cells 2 |
| V1 | the primary visual cortex |
| VEPs | visually evoked potentials |
| ΔF/F | relative changes in fluorescence |

# 1 Introduction

## 1.1 Alzheimer's disease

Alzheimer's disease (AD) is a progressive neurodegenerative disorder and a common cause of cognitive and memory impairment in the elderly. It is estimated that around 50 million patients in the world suffer from this disease and the number of affected people increases over the years (World Alzheimer Report 2018). Not only AD patients suffer from the disease but also their caregivers are suffering from it. Nowadays, AD is one of the most financially costly diseases in developed countries (Alzheimer's Association, 2018).

It has been around 100 years, since AD has been named after Dr. Alois Alzheimer who first described a case of Auguste D., presenting with dementia with an abnormal behaviour. After she passed away in 1906, Alzheimer studied her brain tissue and described the hallmarks of the disease represented by a shrinkage of brain and abnormal deposits, now known as amyloid plaques and neurofibrillary tangles (O'Brien, 1996). At present, pathological hallmarks of AD are (i) the deposition of misfolded and/or aggregating proteins (i.e. amyloid beta (Aβ) plaques and neurofibrillary tangles), (ii) neurodegeneration, (iii) neuroinflammation as well as (iv) neuronal $Ca^{2+}$ dyshomeostasis in extreme cases leading to neuronal death (Goedert and Spillantini, 2006; Holtzman et al., 2011; Palop et al., 2006). Till now AD is still a non-curative disease. Currently available drugs allow only symptomatic treatment. Since these drugs do not target the underlying disease mechanisms, they can improve cognition for a limited time only and do not slow down the disease progression (Cummings et al., 2016; Schneider and Sano, 2009).

Although most of the AD cases occur in patients with the advanced age and an increased age is the main risk factor for AD, AD is not a part of normal healthy ageing. Moreover, around 5 percent of all AD cases have an onset of the disease before the age of 65 years (https://www.alz.org). Thus, AD can be classified into two forms based on the onset of disease (i) Early onset AD and (ii) Late onset AD.

### 1.1.1 Early onset AD

In this form of AD, the majority of patients develop the disease in their 30s to 50s. Most of the cases in the early onset AD are still attributed to unknown causes (Sporadic early onset Alzheimer's disease). However, around 20-30 % of early onset Alzheimer's disease cases inherit AD-associated mutated genes and develop the "Familial Alzheimer's disease or FAD". Mutations in amyloid precursor protein (APP), presenilin 1 (PS1) and 2 (PS2) genes are the most common causes of FAD (Hardy, 1997; Shen and Kelleher, 2007; Steiner and Haass, 2000; Tandon and Fraser, 2002). Out of all known mutations leading to FAD, the majority (more than 100 mutations in total) are located on PS1 (Mattson, 2010). Presenilins are transmembrane proteins which are well-known for being part of the γ-secretase complex. This enzyme plays an important role for APP cleavage and generation of Aβ. On the other side, Presenilins are known to control intracellular $Ca^{2+}$ homeostasis and neurotransmitter release (Bezprozvanny and Mattson, 2008; Chakroborty and Stutzmann, 2014; Hermes et al., 2010; Zhang et al., 2009). AD-mediated mutations in either PS1 or PS2 genes cause an enhancement of γ-secretase activity, resulting in higher amyloid oligomer production and Aβ deposition (Haass, 2004; Jarrett and Lansbury, 1993).

### 1.1.2 Late onset AD

The late onset AD is the most common form of AD (comprising more than 80% of all AD cases), but till now the exact causes of this form are still elusive. Although some non-genetic risk factors such as traumatic brain injury, the history of chronic inflammation, diet and daily activity have been implicated, however, the obvious and well-characterized risk factor in this form is the advancing age. According to twin studies (Gatz et al., 2006), it is suggested that some genetic factors (see below) also might increase the risk of this form of the disease. In contrast to FAD, however, there is no specific mutation predisposing for developing the disease. One of the most well-known risk factors for late onset AD is the apolipoprotein E (ApoE). In the human genome, the ApoE gene has been found in 3 different single-nucleotide polymorphisms which result in 3 different isoforms of ApoE (E2, E3 and E4). People carrying only one allele of E4 isoform have an approximately 4 fold increased risk to develop AD compared to people

with no E4 allele and the risk is increased to 12 fold when carrying two alleles of E4 (Corder et al., 1993; Kim et al., 2009). In addition to ApoE, recent genome wide association studies of the whole exome as well as genome sequencing have identified variants of genes encoding immune receptors as risk factors for AD including triggering receptor expressed on myeloid cells 2 (TREM2), CD33 and complement receptor type 1 (CR1). For example, caucasian people carrying a R45H variance of TREM2 have an approximate 4-5 fold increase risk to develop AD (Colonna and Wang, 2016; Guerreiro et al., 2013; Jonsson et al., 2013).

### 1.2 Neuronal hyperactivity in ageing and Alzheimer's disease

While the deposition of amyloid beta plaques and neurofibrillary tangles are the well-known pathological hallmarks of AD, in recent years neuronal hyperactivity was accepted as the emerging key functional hallmark of AD. The neuronal hyperactivity is often reported in patients with amnestic mild cognitive impairment (aMCI), ApoE4 carriers with an intact cognitive function as well as in AD patients (Bookheimer et al., 2000; Celone et al., 2006; Dickerson et al., 2005; Haberman et al., 2017a; Palop et al., 2006; Palop and Mucke, 2016). The incidence of neuronal hyperactivity, including subclinical epileptiform activity (spikes and sharp waves) is increased in AD patients. Interestingly, the patients with both sporadic and familial forms of AD have a higher propensity to develop seizures (Palop and Mucke, 2016). In addition, fMRI data show an increase in neuronal hyperactivity in the hippocampus of patients with aMCI, which is considered as the preclinical stage of AD, when compared with the age-matched control subjects (Haberman et al., 2017a). Moreover, the degree of neuronal hyperactivity in the hippocampus also correlates with the degree of cognitive impairment in aMCI patients. Additionally, a targeted reduction of neuronal hyperactivity at the postsynaptic terminals with levetiracetam, an atypical antiepileptic drug targeting a synaptic vesicle glycoprotein SV2A, can improve the cognitive impairment in aMCI as well as AD patients (Bakker et al., 2012).

In addition to being a part of the functional hallmarks in AD, neuronal hyperactivity is increasingly observed as a part of ageing, an obvious risk factor of AD. Specifically, Yassa et al. reported that compared to young controls ageing persons performing a pattern separation task show an increase in the neural network activity in the CA3 and dentate gyrus regions of hippocampus (Yassa et al., 2011). This finding was consistent with findings from several animal model studies. For example, Haberman et al. reported an increase in neuronal activity in aged rats (Haberman et al., 2017b; Simkin et al., 2015). In addition, neuronal hyperactivity in the hippocampus was related to memory impairment in aged animals, while low dose administration of levetiracetam, improved memory deficits in aged rats (Koh et al., 2010). Our recent *in vivo* study in the frontal/motor cortex of WT mice revealed that during normal ageing middle-aged (10-14 months old) mice do already reach a substantial level of neuronal hyperactivity (**Figure 1**). Interestingly, the hyperactivity stabilizes at this high level till the end of the animal's life (18 months old; (Lerdkrai et al., 2018; Maier et al., 2014).

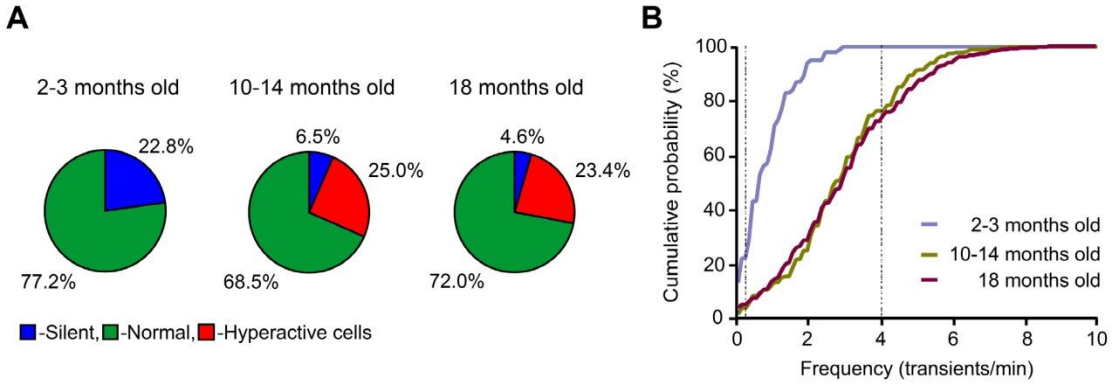


**Figure 1. Development of neuronal hyperactivity in frontal/motor cortex A**, Pie charts illustrating the fractions of silent (blue), normal (green), and hyperactive (red) neurons in the frontal/motor cortex of 3, 10-14 and 18 months old mice. **B**, Cumulative probability functions show the frequency distributions of spontaneous $Ca^{2+}$ transients in the frontal/motor cortex of 10-14 (dark green) and 18 (magenta) months old mice are shifted towards higher frequencies compared to 3 months old mice (purple; $p < 0.01$ for both comparisons, Kolmogorov Smirnov test). Data are acquired by Chommanad Lerdkrai.

### 1.3 Sensory impairment in Alzheimer's disease

Besides the impairment in cognition, an impairment of several sensory systems is a common clinical manifestation in AD patients (Albers et al., 2015). The latter includes olfactory (Daulatzai, 2015; Mesholam et al., 1998), auditory (Gates et al., 2008) and visual processing. Interestingly, olfactory dysfunction is suggested to be one of the earliest clinical manifestations in AD (Devanand et al., 2000). Both aMCI and AD patients show a decreased performance in olfactory identification and recognition (Daulatzai, 2015; Mesholam et al., 1998). Moreover, several studies suggest that this impairment in olfaction could predict the progression of the disease and thus represents a clinical marker of AD (Barresi et al., 2012; Zou et al., 2016). In addition to the olfactory impairment, when compared with age-matched healthy persons aMCI and AD patients show inferior performance in central auditory tests which contain 1) the Synthetic Sentence Identification test with ipsilateral competing message, a monaural speech test with competing message, 2) two dichotic tests involving speech, the Dichotic Sentence Identification test, and the Dichotic Digits test; and 3) the Pitch Pattern Sequence test (Gates et al., 2008).

For the visual processing, it is generally known that the depositing of Aβ plaques and neurofibrillary tangles in the occipital lobe occurs at the late stage of the disease. However, from a functional point of view, both aMCI and AD patients show an alteration of visual processing. Specifically, AD patients show a decrease in contrast sensitivity in all spatial frequency ranges of visual stimuli (Albers et al., 2015; Cronin-Golomb et al., 1991) and are also less capable to detect the direction of visual motion, compared with age-matched controls (Rizzo et al., 2000). Furthermore, visually evoked potentials (VEPs) in AD patients showed a significant reduction of P1 and N1 amplitudes, whereas aMCI patients showed only a reduction of N1 amplitudes (Stothart et al., 2015). In addition, the degree of impairment of contrast selectivity and the abnormal VEPs in both AD and aMCI patients correlated with the degree of their cognitive impairment (Risacher et al., 2013; Rizzo et al., 2000; Stothart et al., 2015).

## 1.4 Neuronal hyperactivity and visual impairment in animal models of Alzheimer's disease

In these days, animal models are important tools for understanding cellular and molecular mechanisms underlying Alzheimer's disease. In general, mice are the most commonly used animal models because compared to other species they are easy to breed and handle with relatively low cost and to manipulate genetically. However, mice do not develop AD pathology by themselves. The generation of mouse models developing AD phenotypes requires either genetic or non-genetic manipulations. The commonly used models are generated by means of genetic manipulations and therefore are called transgenic models. Transgenic models are obtained by integration of known genes, known to cause AD pathology in humans (such as APP or presenilin mutations), into the mouse genome using cell-type specific promoters (Gotz et al., 2018).

Using double transgenic mice with an overexpression of APP with the human Swedish mutation ($APP_{swe}$) and G384A mutation of presenilin 1(PS45) under the Thy-1 promoter, Busche et al. revealed the first *in vivo* evidence for neuronal hyperactivity (Busche et al., 2008). In a study using two-photon $Ca^{2+}$ imaging, the authors discovered in cortical layer 2/3 clusters of neurons exhibiting abnormal activity. Specifically, 21% of all neurons showed an increase in the frequency of spontaneous $Ca^{2+}$ transients ("hyperactive neurons") and 29% showed a decrease in frequency or no spontaneous transients at all ("silent neurons"). Interestingly, the clusters of hyperactive neurons were only found in the areas close to amyloid plaques, whereas silent neurons were equally distributed in the brain parenchyma. Later, neuronal hyperactivity has been described in several other brain regions of different mouse models during either awake or anesthetized states (e.g. hAPP-J20, APP/PSEN1dE9, Tg2576, 5xFAD, 3xTg-AD, APP/TTA-EC, APP/TTA-CaMKIIα, APP23, $APP_{swe}/PS1_{G384A}$, APPPS1, APP/PS1 and hAPPJ9/FYN transgenic mice (Busche et al., 2012; Busche et al., 2008; Maier et al., 2014; Minkeviciene et al., 2009; Palop et al., 2007; Palop and Mucke, 2016; Siskova et al., 2014)).

Using the same animal mouse model of AD ($APP_{SWE}/PS1_{G384A}$ mice) as in the study of Busche et al. (Busche et al., 2008), an *in vivo* imaging of layer 2/3 neurons in

V1 revealed a significant impairment of visual signal processing. Mutant mice were unable to discriminate drifting gratings stimuli. At the cellular level, neurons of mutant mice showed an impairment of orientation and direction tuning properties. Interestingly, this impairment was seen in hyperactive neurons only (Grienberger et al., 2012), while the normal neurons showed orientation and direction tuning properties similar to those of neurons in age-matched control mice, underscoring the relationship between the impairment of visual processing and neuronal hyperactivity.

What is the cause of neuronal hyperactivity in AD? Recent studies have proposed several underlying mechanisms. For example, Busche et al. identified soluble Aβ oligomers as a key factor to promote neuronal hyperactivity in hippocampal CA1 region (Busche et al., 2012). While reducing Aβ by oral treatment of a β-secretase inhibitor ameliorates neuronal hyperactivity in the frontal cortex of $APP_{SWE}/PS1_{G384A}$ mice and improves their memory deficits assessed by water maze test (Keskin et al., 2017). In contrast, Verret et al. reported that a decreased level of a voltage-gated sodium channel subunit Nav1.1, especially in Parvalbumin positive ($PV^+$) interneurons, causes network hypersynchrony and cognitive function deficits. Restoring Nav1.1 level by transgene overexpression in hAPPJ20 mice reduced network hyperactivity and improved learning and memory deficits (Verret et al., 2012). However, the exact cellular/molecular mechanisms of neuronal hyperactivity as well as that of the visual impairment in AD are still elusive.

### 1.5 Role of $Ca^{2+}$ stores for the synaptic transmission in Alzheimer's disease

In addition, $Ca^{2+}$ dyshomeostasis is commonly known as one of the hallmarks of AD. In general, changes of the neuronal intracellular $Ca^{2+}$ concentration $[Ca^{2+}]_i$ are either caused by $Ca^{2+}$ entry through the plasma membrane via voltage-gated and ligand-gated $Ca^{2+}$ channels or by $Ca^{2+}$ release from the intracellular $Ca^{2+}$ stores. The endoplasmic reticulum (ER) is the main intracellular $Ca^{2+}$ source and $Ca^{2+}$ can be released from this store via ryanodine receptors (RyRs) and inositol triphosphate receptors ($IP_3R$). The RyRs are $Ca^{2+}$-activated $Ca^{2+}$ channels, while $IP_3Rs$ are activated

by $IP_3$, a second messenger produced by phospholipase C (PLC) after activation of G-protein coupled receptors in the plasma membrane. The level of $Ca^{2+}$ in the ER is maintained by sarco/endoplasmic reticulum $Ca^{2+}$-ATPases (SERCA pumps), which transport $Ca^{2+}$ from the cytosol into the ER (Berridge et al., 1998; Spat et al., 2008) and the ER leak channels, spontaneously leaking $Ca^{2+}$ into the cytosol (Garaschuk et al., 1997).

Different mechanisms have been proposed to underlie the dysregulation of neuronal $Ca^{2+}$ homeostasis in AD with most studies focusing on Aβ and the mutated PS protein. Various *in vitro* studies have shown that Aβ can nonspecifically enhance $Ca^{2+}$ permeability of both plasma and ER membrane (Bezprozvanny and Mattson, 2008). Furthermore, Aβ has been suggested to form cation-selective ion pores in membranes and to modify endogenous channels permeable for $Ca^{2+}$ (e.g. NMDARs) (Hermes et al., 2010). All these mechanisms lead to increased levels of $[Ca^{2+}]_i$ in the affected neurons. However, the effects of Aβ and other products from APP metabolism on $Ca^{2+}$ homeostasis are still controversial. For example, it has recently been shown in an *in vitro* study that APP has no direct effect on $Ca^{2+}$ regulation (Stieren et al., 2010).

Mutations in PS genes directly change intracellular $Ca^{2+}$ homeostasis in different ways including: (i) sensitizing $IP_3$Rs and RyRs to their agonists, (ii) increasing the expression of both receptors (Cai et al., 2006; Cheung et al., 2008; Guo et al., 1996; Guo et al., 1997; Stutzmann et al., 2006), (iii) increasing $IP_3$ production via enhanced PLC activities (Cedazo-Minguez et al., 2002), (iv) disruption of ER $Ca^{2+}$ leak function leading to $Ca^{2+}$ overfilling of stores (Tu et al., 2006) and (v) enhancing SERCA pump activities (Green et al., 2008).

Our recent *in vivo* study in the frontal/motor cortex of both $APP_{SWE}/PS1_{G384A}$ and $PS1_{G384A}$ mice (Lerdkrai et al., 2018) revealed an important role of the presynaptic intracellular $Ca^{2+}$ stores for controlling amplitude and frequency of axonal $Ca^{2+}$ transients in presynaptic boutons in both mouse strains. Interestingly, only a single allele of G384A mutation was enough to develop neuronal hyperactivity without the deposition of amyloid plaques and neuroinflammation. This is likely due to a presenilin-mediated dysfunction of intracellular $Ca^{2+}$ stores in presynaptic boutons causing an

increase in neurotransmitter release and an increased NMDA receptor activation in the postsynaptic neurons. In the somato-dendritic compartment of layer 2/3 neurons we found a slight overfilling of the intracellular $Ca^{2+}$ stores exclusively in hyperactive cells, and this overfilling was much smaller than what can be inferred from the *in vitro* data (Goussakov et al., 2010). Moreover, emptying the intracellular $Ca^{2+}$ stores with cyclopiazonic acid (CPA), a reversible SERCA blocker, as well as blocking the ryanodine receptors with dantrolene caused a significant reduction of neuronal hyperactivity in these mutant mice.

Taken together, neuronal hyperactivity is recognized as the one of functional hallmarks of AD as well as healthy ageing, and an obvious risk factor for AD. Previous study suggested the relationship between neuronal hyperactivity and the impairment of the visual processing in AD mice. However, the degree of the impairment and the cellular mechanisms involved in AD as well as the link between neuronal hyperactivity and visual processing in healthy ageing are still elusive. In the present study, we first characterized the effect of ageing on the processing of visual stimuli by V1 neurons. Subsequently, animal models of AD were used to characterize in detail on AD-related changes in the visual tuning properties. Lastly, using the newly developed treatment protocol for reduce store-mediated neuronal hyperactivity we tested whether this treatment is able to ameliorate the deficits in visual processing in mouse models of AD.

## 1.6 Aims of this project

The aim of this project was:

1. To study age-related changes in visual response properties during normal ageing.

2. To understand the relationship between the impairment of visual processing and neuronal hyperactivity.

3. To test whether reducing store-mediated neuronal hyperactivity is also able to ameliorate the deficits in visual processing.

4. To characterize in detail alterations of visual processing in $APP_{SWE}/PS1_{G384A}$ as well as $PS1_{G384A}$ mice

# 2 Materials and methods

## 2.1 Animals

All experiments were conducted in accordance with institutional animal welfare guidelines and were approved by the state government of Baden-Württemberg, Germany. To study age-related changes in neuronal properties, C57Bl/6 (WT) mice were used at the age of 3, 10-12 and 18 months. In order to study AD related functional changes in the visual processing, 10-12 months old $APP_{swe}/PS1_{G384A}$ mice (AD mice) were used. This mouse model of AD shows a robust plaque deposition starting from 2-3 months of age and an impairment of memory performance, assessed by water maze and Y maze tests, was observed in this mouse model at the age of 6-8 months. 10-12 months old heterozygous $PS1_{G384A}$ mice (PS45 mice) were used to study the role of presenilin mutation alone. Both mouse models were raised on the C57Bl/6 background and transgenes were expressed selectively in neurons under control of the Thy-1 promoter (Busche et al., 2008). Age-matched WT mice were used as wild-type controls. All experiments were performed in animals of mixed sex. Female animals were maintained in groups of 3-5 mice. Male animals were maintained individually. Animals were kept under a 12 hours light/dark cycle and were fed ad libitum.

## 2.2 Surgical procedure

Animals were anesthetized using isoflurane (1.5% in pure oxygen during surgery and 0.8-1% in pure oxygen during recording) and kept on a warming plate. The respiratory rate and the body temperature were continuously monitored and kept at 100-150 breaths per minute and 37º C , respectively. Skin removal above V1 (-2.5 to -3.5 mm posterior to bregma and 2-3 mm lateral to midline) was performed after a subcutaneous injection of 2% lidocaine (Sanofi-Aventis, Frankfurt, Germany). The skull was thinned using a dental drill (NSK, Eschborn, Germany) and a custom-made recording chamber (**Figure 2A**) was fixed to the skull (**Figure 2B**) using cyanoacrylate glue (UHU, *Bühl, Germany*). Subsequently, the animal was moved into the imaging setup and the chamber was continuously perfused with warm (37 °C) extracellular fluid containing (in mM): 125 NaCl, 4.5 KCl, 26 $NaHCO_3$, 1.25 $NaH_2PO_4$, 2 $CaCl_2$, 1 $MgCl_2$,

20 glucose, pH 7.4 (when bubbled with 95% $O_2$ and 5% $CO_2$). A small craniotomy (≤ 1 $mm^2$) was performed above the V1 using a 30G needle. Animals were subcutaneously injected with warm (37 °C) extracellular fluid every 2 hours for maintaining the physiological conditions (Eichhoff and Garaschuk, 2011; Garaschuk et al., 2006).

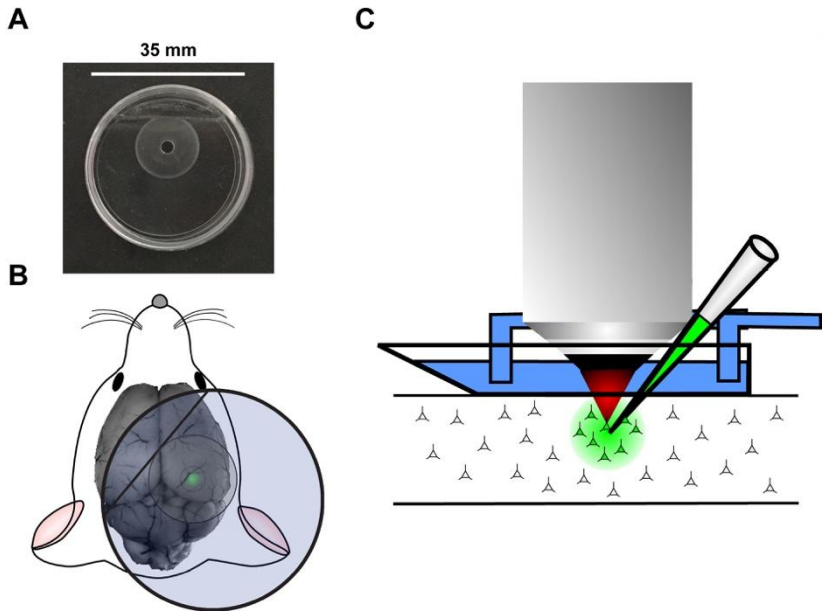


**Figure 2. Schematic illustration of the experimental set up for *in vivo* $Ca^{2+}$ imaging in the primary visual cortex. A,** An example of a custom-made recording chamber which was specially designed for current experiments. **B,** A schematic representation of the top view on a mouse brain where a rotated recording chamber is mounted above V1. The drawing of the mouse was obtained from Chommanad Lerdkrai. **C,** A schematic illustrates a side view of experimental setup during labeling of neurons with the multi-cell bolus loading technique (modified from (Garaschuk et al., 2006)).

## 2.3 *In vivo* two-photon $Ca^{2+}$ imaging

*In vivo* two-photon imaging was performed with a custom-built two-photon microscope (Olympus Fluoview, Olympus) coupled to a mode-locked Ti-Sapphire laser working at a wavelength of 710-990 nm (MaiTai, Spectra Physics). All images were taken with a water-immersion objective (Nikon 40x, 0.8 NA).

Neurons were labeled with a small molecule $Ca^{2+}$ indicator Cal-520-AM (Tada et al., 2014) by means of the multi-cell bolus loading technique (Garaschuk et al., 2006;

Stosiek et al., 2003). Cal-520-AM was dissolved in 20% Pluronic F-127 (Molecular Probes, Oregon, USA) solution (in DMSO) and was further diluted with a standard pipette solution (150 mM NaCl, 2.5 mM KCl, 10 mM HEPES (pH 7.4)), giving the final dye concentration of 0.5 mM. The solution was pressure-injected (70 kPa for 2 min) into the brain parenchyma approximately 150-200 µm below the dura (**Figure 2C**). After one hour, the dye was fully taken up by neurons and astrocytes. Astrocytes could be easily distinguished from neurons by their bright appearance and cell-type-specific morphology. The Cal-520-labeled neurons were imaged using an excitation wavelength of 800 nm. Spontaneous $Ca^{2+}$ signaling was monitored for a total of 6 min and visually-evoked $Ca^{2+}$ signaling was monitored for a total of 18 min. Both measurements were conducted at a frame rate of 7.7 Hz.

## 2.4 Visual stimulation

### 2.4.1 Experimental setup

Visual stimuli were generated with the 'Psychtoolbox' (https://psychtoolbox.org/HomePage) add-on package in Matlab (The Mathworks). The stimuli were projected onto a screen, which was placed 30 cm from the contralateral eye covering 80° x 60° of the visual field, as shown in **Figure 3**. The line scan signal from the microscope was used to trigger the visual stimulation. Hence, the start of the two-photon $Ca^{2+}$ imaging was synchronized with the start of the visual stimulation.

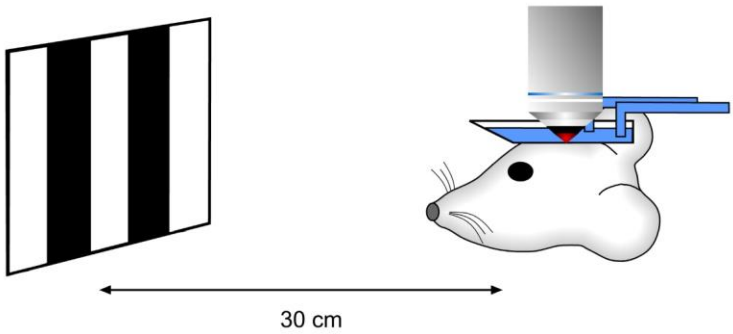

**Figure 3. Schematic representing the experimental setup for two-photon $Ca^{2+}$ imaging of visual-evoked response.** The right image illustrates a side view of the recording chamber attached to the mouse skull. The chamber was continously perfused with the extracellular fluid. In some experiments, CPA and dantrolene were added to the extracellular fluid continously perfusing the chamber ("Bath application"). The drawing of the mouse was obtained from Chommanad Lerdkrai.

### 2.4.2 Visual stimulation protocol

Neurons were stimulated by square-wave drifting gratings with 100% contrast, 0.03 cycles per degree and 1.5 Hz temporal frequency. The standard stimulation protocol started with a grey screen for 6 s (baseline condition), followed by static gratings for 6 s, a grey screen for 6 s and drifting gratings for 4 s. In each trial (6 trials in total) this protocol was repeated 8 times for 8 different directions of drifting gratings (**Figure 4**).

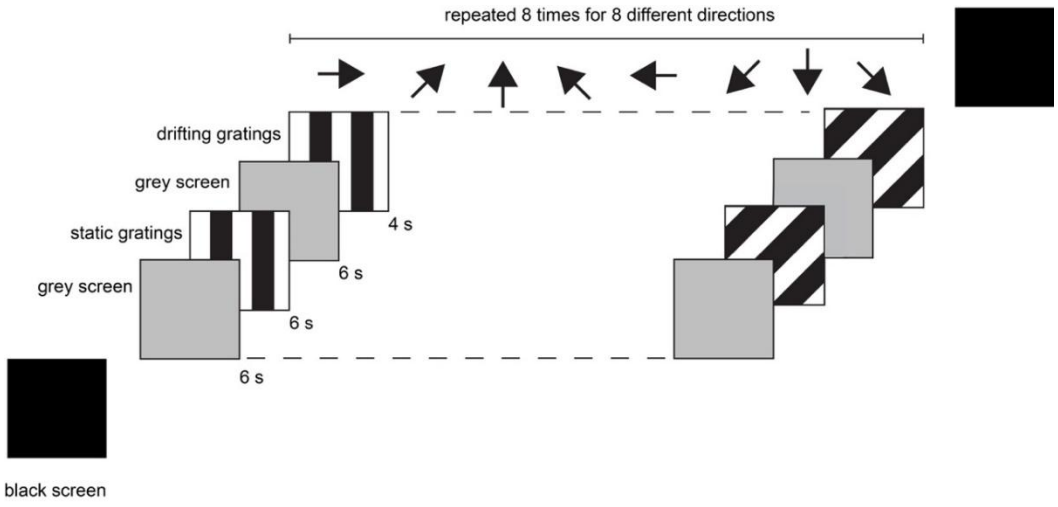


**Figure 4. Schematic illustration of the standard visual stimulation protocol**

## 2.5 Data analyses

Data analysis was performed offline with Image J (http://imagej.nih.gov/ij/), custom-made routines of Igor Pro (Wavemetrics) and Matlab (The Mathworks). If not

otherwise indicated, data is presented as median ± interquartile range. Lines of boxes represent 25th and 75th, and whiskers 10th and 90th percentiles.

### 2.5.1 Analysis of ongoing spontaneous activity

For measurements of neuronal activity, we first read out the fluorescence intensity from regions of interest (ROIs) drawn around individual cell bodies and a background ROI, placed within a large blood vessel. Background-subtracted fluorescence intensity values were then used to calculate relative changes in fluorescence (ΔF/F) for individual neurons. A change in ΔF/F was considered as a $Ca^{2+}$ transient when its amplitude was higher than threefold the standard deviation (SD) of the corresponding baseline noise. Baseline noise was computed by subtracting a strongly low pass filtered (moving average method) trace from the original signal. According to the frequency of their spontaneous $Ca^{2+}$ transients, recorded neurons were classified as silent (0-0.25 transients/min), normal (0.26-4 transients/min) or hyperactive (> 4 transients/min) neurons similar to the previous literature (Busche et al., 2008; Grienberger et al., 2012; Lerdkrai et al., 2018).

### 2.5.2 Analysis of visually evoked activity

A neuron was considered visually responsive when the maximum ΔF/F of the averaged trace (mean of 6 trials) was higher than threefold the SD of the corresponding baseline noise. In this study we measured the neuron's responsiveness to 3 different visual stimuli: (i) drifting gratings, (ii) static gratings ON, measured during the beginning of the respective stimulus and (iii) static gratings OFF, measured 0-200 ms after switching off the respective stimulus (**Figure 5**).

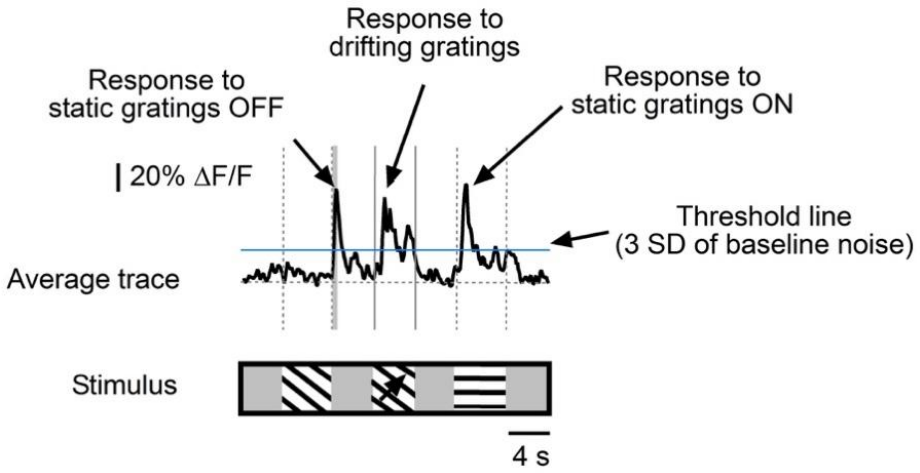


**Figure 5. A representative example of an average trace (from 6 trials) of visually evoked neuronal response recorded from a Cal-520 AM labeled neuron. Arrows indicate neuronal response to 3 different visual stimuli.**

In addition, the main findings of the study were verified by using an alternative technique for identification of visually responsive-neurons (as described in (Chen et al., 2013)). In the latter case (i) neuropil signal was estimated by averaging fluorescence signals of all pixels located outside the cell bodies (in ≥ 4 months old WT animals activity-dependent neuropil signal is generally negligible but might get larger in plaque-depositing AD mice (Busche et al., 2008)), (ii) $F_{cell\_measured}$ fluorescence signals were read out from ROIs drawn around individual cell bodies, (iii) the fluorescence signals of all cell bodies were corrected for a possible neuropil contamination by calculating $F_{cell\_true}(t) = F_{cell\_measured}(t) - 0.7 \times F_{neuropil}(t)$. Visually responsive-neurons were defined as cells with significant stimulus-related fluorescence changes (ANOVA across presentation of the grey screen and either 8 directions of drifting gratings stimuli or 4 orientations of ON/OFF stimuli, $p<0.01$, see also (Chen et al., 2013)). Please note that the second technique for identification of visually responsive-neurons is less sensitive compared to the first one because of the higher noise of individual traces compared to the average trace.

Direction and orientation selectivity were determined by direction (DSI) and orientation (OSI) selectivity indices (Niell and Stryker, 2008). The OSI is defined as $(R_{pref} - R_{ortho})/(R_{pref} + R_{ortho})$ and DSI is defined as $(R_{pref} - R_{opp})/(R_{pref} + R_{opp})$, where $R_{pref}$

is the area under the ΔF/F transient recorded during the presentation of the preferred orientation or direction. $R_{ortho}$ is the area under the ΔF/F transient recorded during the presentation of the orientation, orthogonal to $R_{pref}$. $R_{opp}$ is the area under the ΔF/F transient recorded during the presentation of the direction, opposite to the preferred direction. Circular variance was calculated as $= 1 - \left|\frac{\sum R_k e^{2i\theta_k}}{\sum R_k}\right|$, where $R_k$ is the area under the ΔF/F transient recorded during the presentation of drifting gratings at an angle $\theta_k$, with $\theta_k$ ranging in our case from 0º to 360º in 45º steps (see also (Niell and Stryker, 2008)).

Activity ratio was calculated for each visually responsive-neuron by dividing the frequency of $Ca^{2+}$ transients, recorded during the presentation of the grey screen (recording started 200 ms after grey screen ON and ended with grey screen OFF) by the frequency of $Ca^{2+}$ transients, recorded before the presentation of the visual stimuli (i.e. during black screen).

### 2.6 Statistical analyses

For each experiment the choice of the sample size was based on biometrical sample size estimation. Statistics was performed using the GraphPad Prism 6 software (GraphPad Software, Inc.) and IBM SPSS Statistics (IBM Corporation). One-sample Kolmogorov-Smirnov test was used for assessing normality of data distribution. Two-sample Kolmogorov-Smirnov test was used for comparing two data distributions. Comparisons between two dependent variables were performed using the Wilcoxon-Signed-Rank test. Kruskal-Wallis test, followed by Dunn's post hoc test, was used for comparing three independent groups. Visually responsive-neurons were identified using ANOVA. Two-way repeated measures ANOVA (rANOVA) with one between (mouse strains) and one within factor (control vs. treatment in the same animal) and F-tests followed by Fisher's LSD test was used for testing the effect of two independent factors within the same data set. In the regression analyses used for estimating the relationships between visual tuning properties (as measured by DSI, OSI, and circular variance) and the frequency of spontaneous activity, the dependency of measurements

was adjusted for by Generalized Estimating Equations (GEE, (Zeger and Liang, 1986), with exchangeable correlation structure. The values of the correlation coefficients given in the legend of **Figure 22** are purely descriptive, p-values refer to the GEE analysis. Differences were considered significant if $p < 0.05$.

### 2.7 Establishing treatment protocol for store depletion

To study the role of intracellular $Ca^{2+}$ stores *in vivo*, CPA (Enzo Life Sciences, New York, USA) and dantrolene (Sigma-Aldrich, St. Louis, USA) were first dissolved in DMSO and then the solution was diluted again with the extracellular fluid to reach the final concentration (400 µM for CPA and 100 µM for dantrolene). The ready-to-use drug-containing solution was used to perfuse the recording chamber as shown in **Figures 3** ('bath application') for 30 min prior to recording the drug effect. This CPA application technique completely abolishes caffeine-induced $Ca^{2+}$ release form the intracellular stores *in vivo* (Lerdkrai et al., 2018).

First, we tested the effect of CPA on spontaneous neuronal $Ca^{2+}$ transients in the frontal/motor cortex of PS45 and AD mice. In addition to frequency of spontaneous $Ca^{2+}$ transients, amplitude, T-half and Tau of spontaneous $Ca^{2+}$ transients were measured as shown in **Figure 6**.

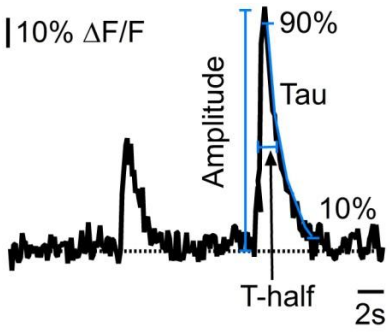


**Figure 6. A representative example of trace of spontaneous $Ca^{2+}$ transient recorded from a Cal-520 AM labeled neuron. Arrows indicate parameters, measured in this study.**

Emptying the intracellular $Ca^{2+}$ store with bath application of CPA significantly reduced the frequency of ongoing spontaneous $Ca^{2+}$ transients in normal and

hyperactive neurons in both PS45 and AD mice without affecting WT mice. In addition, CPA has no effect on the shape of the shape of spontaneous $Ca^{2+}$ transients (**Figure 7**).

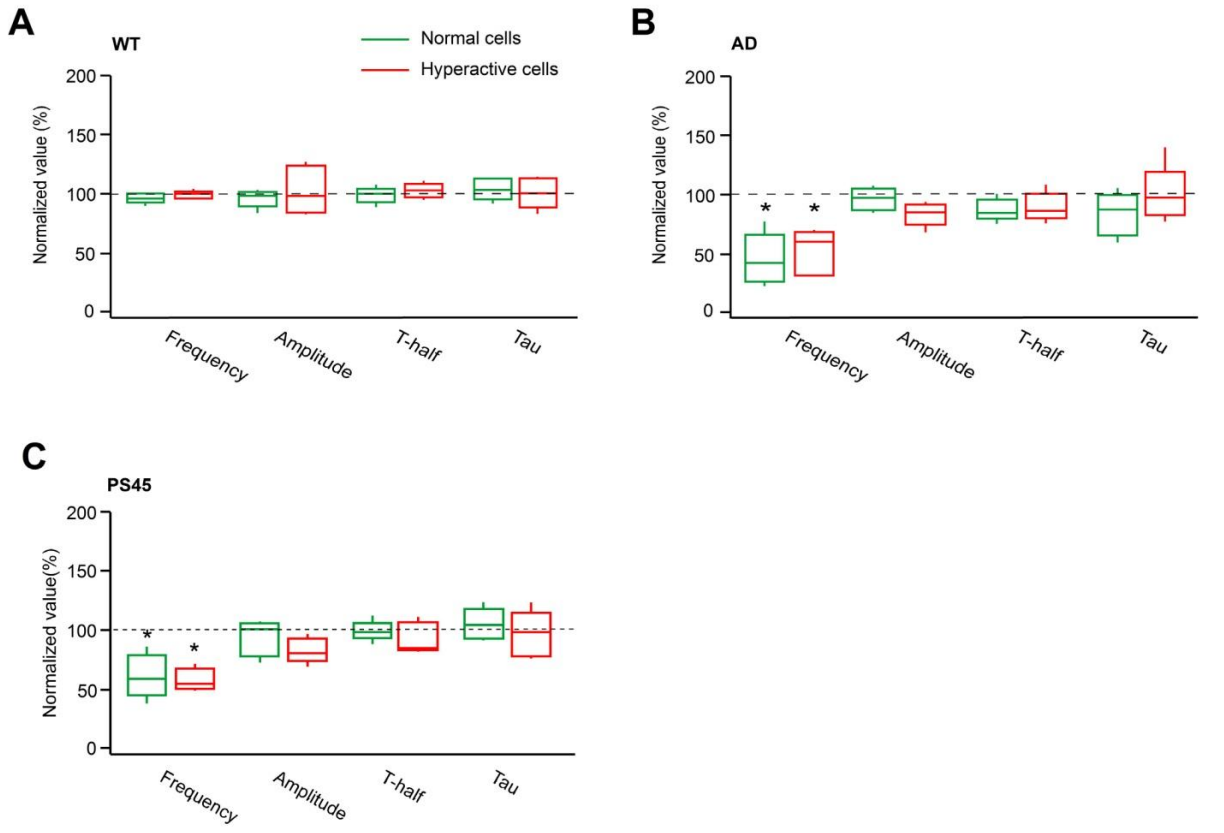


**Figure 7. Emptying intracellular $Ca^{2+}$ with CPA reduce neuronal hyperactivity in AD and PS45 mice.** Box-and whisker plots illustrating the effect of CPA on median frequency, amplitude, T-half, and tau of spontaneous $Ca^{2+}$ transients recorded from normal (green) and hyperactive (red) cells in WT (**A**), AD (**B**), and PS45 (**C**) mice. All values measured under CPA are normalized to respective control values. CPA significantly reduced the frequency of spontaneous transients in normal and hyperactive cells in AD and PS45 mice (two-way rANOVA; $p < 0.01$ for all comparisons) without effecting WT mouse (two-way rANOVA; $p = 0.78$). n = 5, 5, 5 mice for WT, AD and PS45 mice, respectively. Data were acquired by Chommanad Lerdkrai.

Moreover, similar results were obtained when blocking the ryanodine receptors with dantrolene, however dantrolene significantly reduced the frequency of ongoing spontaneous $Ca^{2+}$ transients only in the hyperactive neurons of all mouse strains (**Figure 8**).

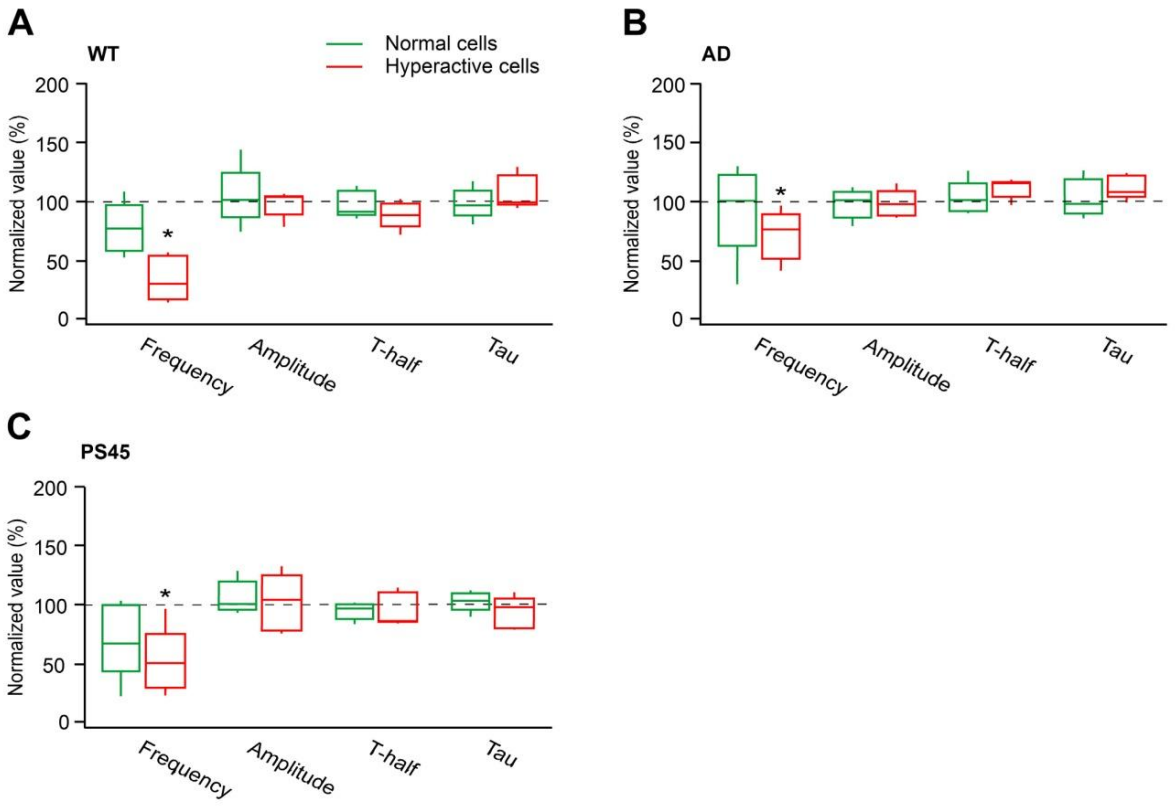


**Figure 8. Ryanodine receptor blocker dantrolene reduces the frequency of spontaneous $Ca^{2+}$ transients in hyperactive cells in frontal/motor cortex**. Box-and whisker plots illustrating the effect of dantrolene on median frequency, amplitude, T-half, and tau of spontaneous $Ca^{2+}$ transients recorded from normal (green) and hyperactive (red) cells in WT (**A**), AD (**B**), and PS45 (**C**) mice. All values measured under dantrolene are normalized to respective control values. Dantrolene significantly reduced the frequency of spontaneous transients in hyperactive cells in all mouse strains (two-way rANOVA; $p < 0.01$ for WT, $p = 0.03$ for AD and $p < 0.01$ for PS45). n = 5, 5, 5 mice for WT, AD and PS45 mice, respectively.

Based on the above data we concluded that both CPA and dantrolene are able to reduce the pathological activity of the hyperactive neurons, thus pointing to the important contribution of the intracellular $Ca^{2+}$ stores to neuronal hyperactivity. However, only CPA selectively reduced hyperactivity in the mouse models of AD only, whereas dantrolene reduces both AD- and ageing-induced hyperactivity. Therefore, we chose to use CPA in the following studies (see below).

# 3 Results

## 3.1 Age-related changes of neuronal properties in the primary visual cortex of WT mice

### 3.1.1 Age-related increase in neuronal hyperactivity

It is a generally known that ageing is the one of the major risk factors for AD. Our recent study showed that neurons in the frontal/motor cortex of middle-aged mice (10-12 months old) exhibited a significant age-related change in neuronal hyperactivity (Lerdkrai et al., 2018). However, the changes of neuronal properties in the V1 during ageing still remain unclear. To obtain a proper control for the subsequent AD studies we first characterized ageing-related changes in neuronal properties in V1. The latter were characterized during 3 different phases of life (3 (young adult), 10-12 (middle-aged) and 18 (aged) months old mice).

Layer 2/3 neurons in V1 of 3, 10-12 and 18 months old WT mice were labeled with a small molecule $Ca^{2+}$ indicator Cal-520 (Tada et al 2014). The ongoing spontaneous $Ca^{2+}$ transients of layer 2/3 neurons in the primary visual cortex of 3, 10-12 and 18 months old WT mice were first analyzed as described in Materials and methods section and all recorded neurons were classified as silent, normal or hyperactive (**Figure 9**).

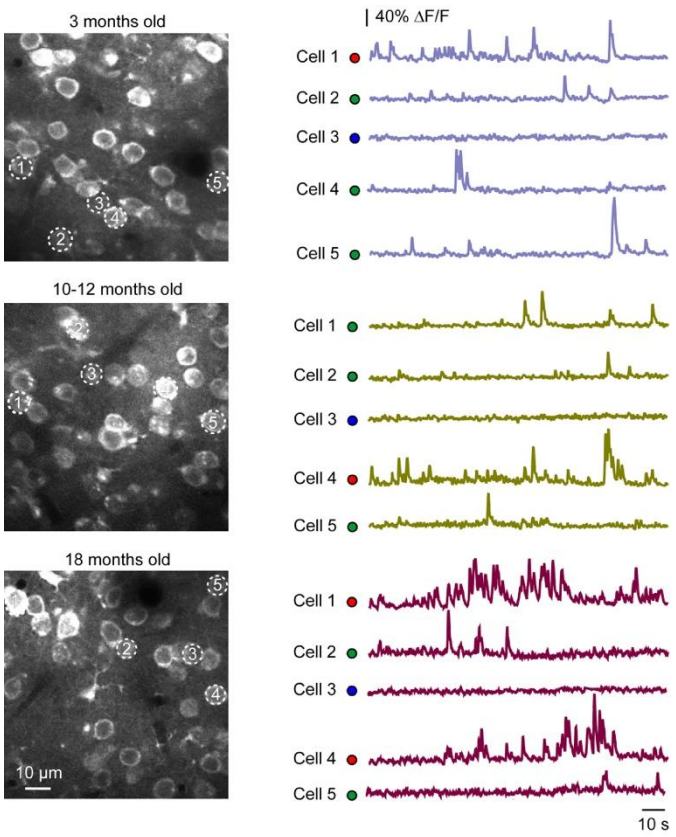


**Figure 9. *In vivo* measurements of spontaneous neuronal activity in 3, 10-12 and 18 months old WT mice.** Left, maximum intensity projection (MIP) images of layer 2/3 neurons in the primary visual cortex of a 3 (top), 10-12 (middle) and 18 (bottom) months old mouse. Right, spontaneous $Ca^{2+}$ transients recorded simultaneously from neurons marked with respective numbers in the corresponding left panel. Here and below, the dots in front of the traces are color-coded according to the frequency of spontaneous $Ca^{2+}$ transients: blue for silent, green for normal, and red for hyperactive cells.

The fraction of hyperactive neurons in layer 2/3 of V1 of 3 months old WT mouse was higher when compared with layer 2/3 of frontal/motor cortex with the same age (compare **Figure 10A** to **Figure 1A**). The fraction of hyperactive neurons in layer 2/3 of V1 showed a tendency to increase from 16.7% at 3 months to 22.5% at 10-12 months, however it didn't reach a significant level ($p = 0.17$, chi square test) and the fraction of hyperactive neurons was increased significantly to 34.9% at the age of 18 months ($p < 0.01$ for 3 vs. 18 months old, $p < 0.01$ for 10-12 vs. 18 months old, chi square test). The frequency distribution of ongoing spontaneous $Ca^{2+}$ transients and median (per mouse) spontaneous $Ca^{2+}$ transients in 18 months old mice was significantly higher, compared to that recorded from 3 and 10-12 months old mice (**Figure 10 B,C**).

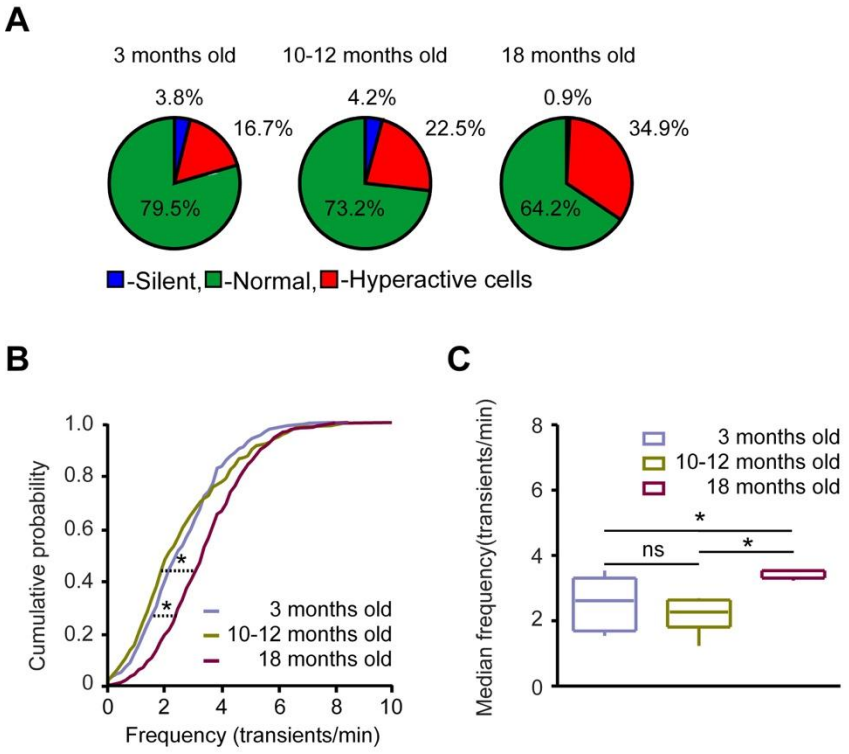


**Figure 10. Age-related increase in neuronal hyperactivity in V1. A**, Pie charts illustrating the fractions of silent, normal, and hyperactive neurons in the primary visual cortex of 3, 10-12 and 18 months old mice. **B**, Cumulative probability distributions showing the frequency of spontaneous $Ca^{2+}$ transients in V1. Distribution of 18 months old mice is shifted towards higher frequencies compared to 3 and 10-12 months old mice ($p < 0.01$ for both comparisons, Kolmogorov Smirnov test). **C**, box-and-whisker plot showing the median (per mouse) frequency of spontaneous $Ca^{2+}$ transients in a 3 (purple), 10-12 (dark green) and 18 (magenta) months old mice. The median frequencies in 18 months old mice are significantly higher compared to 3 and 10-12 months old mice ($p = 0.048$ for 3 vs. 18 months old, $p < 0.01$ for 10 vs. 18 months old and $p = 0.48$ for 3 vs. 10 months old, Kruskal-Wallis test). 3 months old: n = 312 neurons from 5 mice; 10-12 months old: n = 306 neurons from 6 mice; 18 months old: n = 375 neurons from 6 mice.

### 3.1.2 Changes in visual response properties during ageing

Visually-evoked $Ca^{2+}$ transients in layer 2/3 neurons in V1 were caused by visual stimuli, projected on a screen placed at a 30 cm distance from the contralateral eye. A schematic of the experimental set up is shown in **Figure 3**. **Figure 11** shows three consecutive trials as well as the corresponding averaged traces, recorded from representative visually responsive-neurons (marked with arrowheads on a respective

left panel) in 3 (top), 10-12 (middle) and 18 (bottom) months old mice. The fraction of layer 2/3 neurons in V1 responding to drifting gratings stimuli among 3 age groups were similar (**Table 1**).

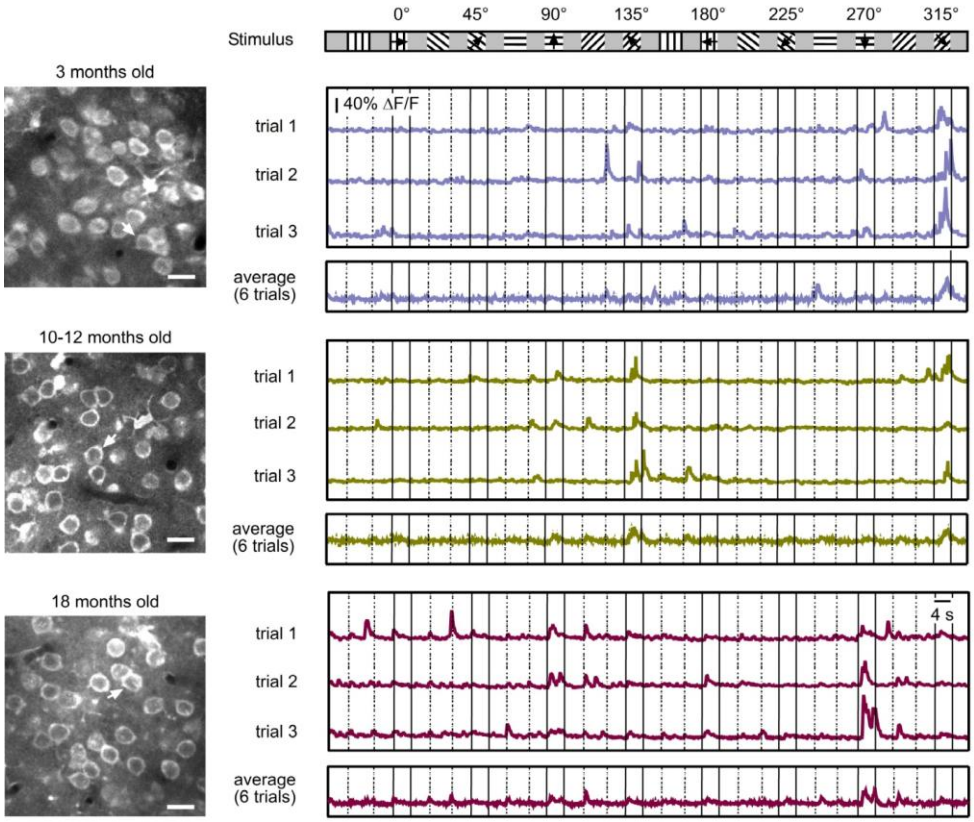


**Figure 11. Visual response properties during ageing.** Left, MIP images of layer 2/3 neurons in V1 of a 3 (top), 10-12 (middle) and 18 (bottom) months old mouse, respectively. Right, three representative traces and an average of six trials recorded from neurons marked with arrowheads in the corresponding left panel, in response to standard stimulation protocol.

| | **Drifting-gratings stimuli** |
|---|---|
| **3 months old** | 57.0±23.2% |
| **10-12 months old** | 46.3±12.4% |
| **18 months old** | 47.9±23.0% |

**Table 1. Summary of the fraction of neurons responding to drifting-gratings stimuli in 3, 10-12 and 18 months old WT mice.** The fraction of layer 2/3 neurons in V1 responding to drifting grating stimuli were similar among 3 age groups (p = 0.77, Kruskal-Wallis test; n = 5, 6, 6 mice for 3, 10-12 and 18 months old WT mice, respectively).

Further, AUC of $Ca^{2+}$ transients evoked by the preferred and non-preferred directions (**Figure 12A, B**) as well as the preferred and non-preferred orientations (**Figure 12C, D**) of drifting gratings stimuli were analyzed. The visually responsive-neurons among the 3 age groups showed similar AUCs of $Ca^{2+}$ transients evoked by all preferred direction, non-preferred directions, preferred orientation and non-preferred orientations (**Figure 12**).

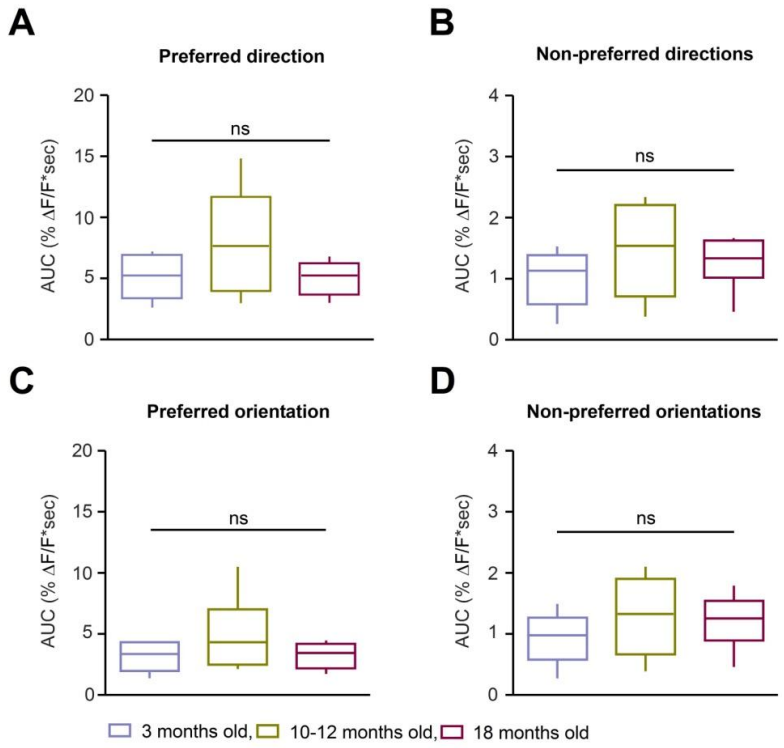


**Figure 12. Similar area under the curve (AUC) of $Ca^{2+}$ transients evoked by visual stimuli in 3, 10-12 and 18 months old mice. A-D**, box-and-whisker plots showing the median (per mouse) areas under the curve (AUCs) of neuronal responses evoked by the preferred direction (**A**), non-preferred directions (**B**), preferred orientation (**C**) and non-preferred orientations (**D**) of drifting gratings stimuli in 3 (purple), 10-12 (dark green) and 18 (magenta) months old mice. There was no significant difference in AUCs of neuronal responses evoked by the preferred direction, non-preferred directions, preferred orientation and

non-preferred orientations among 3 age groups ((**A**) p = 0.69, (**B**) p = 0.53, (**C**) p = 0.69, (**D**) p = 0.41, Kruskal-Wallis test). n = 5, 6 and 6 mice for 3, 10-12 and 18 months old, respectively.

At the single cell level, layer 2/3 neurons of V1 in WT mice exhibit highly direction- and orientation-selective tuning, which can be described quantitatively by DSI and OSI (Niell and Stryker, 2008). To test visual tuning properties of visually responsive-neurons during ageing, the DSI (**Figure 13A**) and OSI (**Figure 13B**) of the visually responsive-neurons were compared in the 3 different age groups (3, 10-12 and 18 months old animals). Mice at the age of 18 months showed a decrease in orientation tuning when compared to OSI of the visually responsive-neurons recorded from 3 and 10-12 months old mice while OSI of the visually responsive-neurons recorded from 3 and 10-12 months old mice were similar (**Figure 13B**). DSI of the visually responsive-neurons were similar among the 3 age groups (**Figure 13A**).

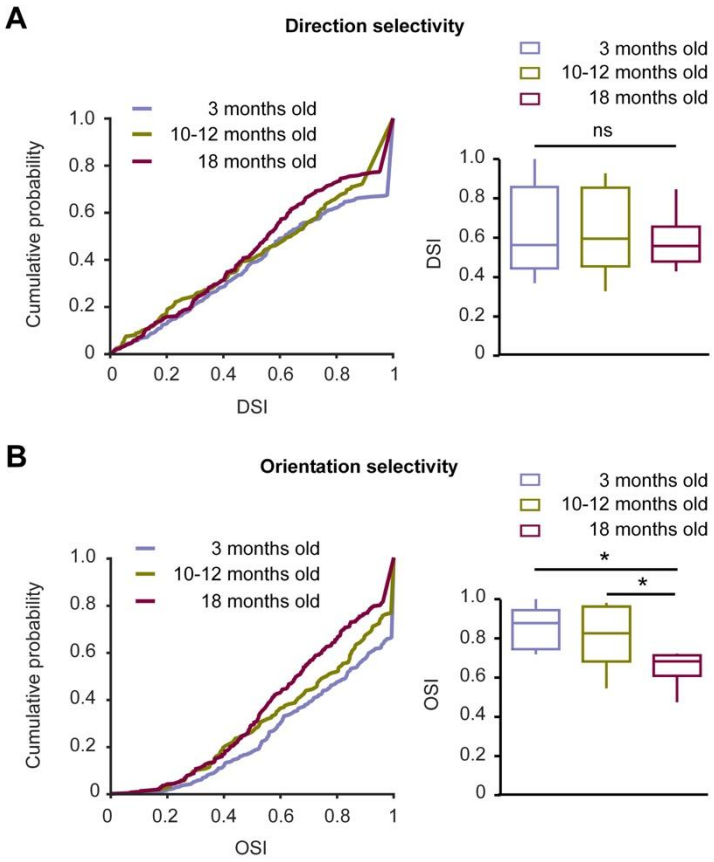

**Figure 13. Decreased orientation selectivity during ageing. A, B** Left: cumulative probability distributions of direction (DSI) and orientation (OSI) selectivity indices of neurons in 3, 10-12 and 18 months old mice. Right: box-and-whisker plots showing the median (per mouse) DSI (**A**) and OSI (**B**) values in different age groups. Median OSI in 18 months old mice is significantly lower compared to 3 and 10-12 months old mice (p = 0.01 for 3 vs. 18 months old, p = 0.03 for 10-12 vs. 18 months old and p = 0.65 for 3 vs. 10-12 months old, Kruskal-Wallis test) while the median DSIs are similar among 3 groups (p = 0.90, Kruskal-Wallis test).

Next, the $Ca^{2+}$ transients in response to drifting gratings of different angles were plotted for visualizing the overall visual response properties among the 3 age groups (**Figure 14A**). The visually responsive-neurons in 18 months old mice (**Figure 14A**, right) showed a wider response function to oriented drifting gratings than visually responsive-neurons in 3 (**Figure 14A**, left) and 10-12 (**Figure 14A**, middle) months old mice. However, when the circular variance is calculated, the difference did not reach the level of statistical significance (**Figure 14B**).

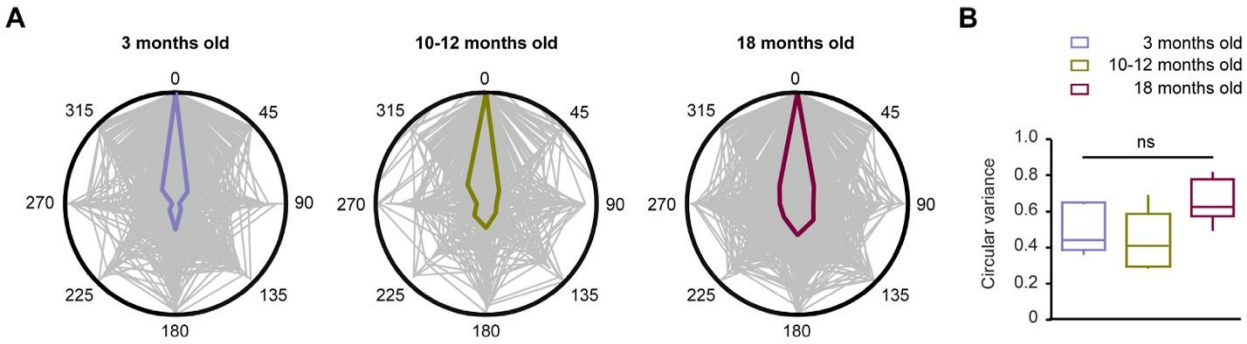


**Figure 14. Response function to oriented drifting gratings in 3, 10-12, 18 months old WT mice. A**, polar plots showing response functions of all neurons (grey) to oriented drifting gratings in 3, 10-12 and 18 months old mice. The medians of neuronal responses in 3, 10-12 and 18 months old mice are shown as purple, dark green and magenta lines, respectively. **B,** box-and-whisker plot showing the median (per mouse) circular variance values of in 3 (purple), 10-12 (dark green) and 18 (magenta) months old mice. The median circular value among 3 groups are similar (p = 0.10, Kruskal-Wallis test). n = 5, 6 and 6 mice for 3, 10-12 and 18 months old mice, respectively.

Taken together, these results show a development of neuronal hyperactivity in layer 2/3 of V1 during normal ageing which mimics the previous finding in layer 2/3 of frontal/motor cortex. However, the increase in neuronal hyperactivity in layer 2/3 of V1 developed later (18 months old of age), while neuronal hyperactivity in layer 2/3 of the frontal/motor cortex developed earlier at the age of 10-14 months and remained high till

the age of 18 months. In addition to an increased neuronal hyperactivity in 18 months old mice, visually responsive-neurons decreased their orientation tuning property without changing their direction tuning property and circular variance.

### 3.2 A profound neuronal hyperactivity in the primary visual cortex of both $PS1_{G384A}$ and $APP_{swe}/PS1_{G384A}$

For studying mechanisms underlying AD-related functional alterations of visual processing, AD mice were chose the middle-aged mice (10-12 months of age). Because at this age AD mice show a robust plaque deposition and significant learning and memory deficits (Busche et al., 2008; Grienberger et al., 2012; Lerdkrai et al., 2018). Because neuronal properties (spontaneous activity and visual tuning properties) in 10-12 months old mice are similar to that found in young adult mice (3 months old, see above), choosing this age group we were able to study the effect of AD-related mutation alone without interfering with the effect of ageing. The 10-12 months old PS45 mice were used for studying the role of G384A mutation alone. As was shown in our previous study (Lerdkrai et al., 2018), these mice show neither amyloid deposition nor neuroinflammation.

Layer 2/3 neurons in V1 of 10-12 months old WT, PS45 and AD mice were labeled with a small molecule $Ca^{2+}$ indicator Cal-520 (Tada et al 2014) as described above and the ongoing spontaneous activity of these labeled neurons was analyzed. **Figure 15A** shows representative recordings of spontaneous $Ca^{2+}$ transients from neurons in WT (top, the recorded neurons are marked with respective numbers in the left panel), PS45 (middle) and AD (bottom) mice. Similar to our previous findings in the frontal/motor cortex (Lerdkrai et al., 2018), the frequency distributions of spontaneous $Ca^{2+}$ transients recorded in V1 of PS45 and AD mice were significantly shifted to higher frequencies, compared to the frequency distribution found in WT mice (**Figure 15B**). The median (per mouse) frequencies of spontaneous $Ca^{2+}$ transients in PS45 and AD mice were also significantly higher, compared to that found in WT mice (**Figure 15C**).

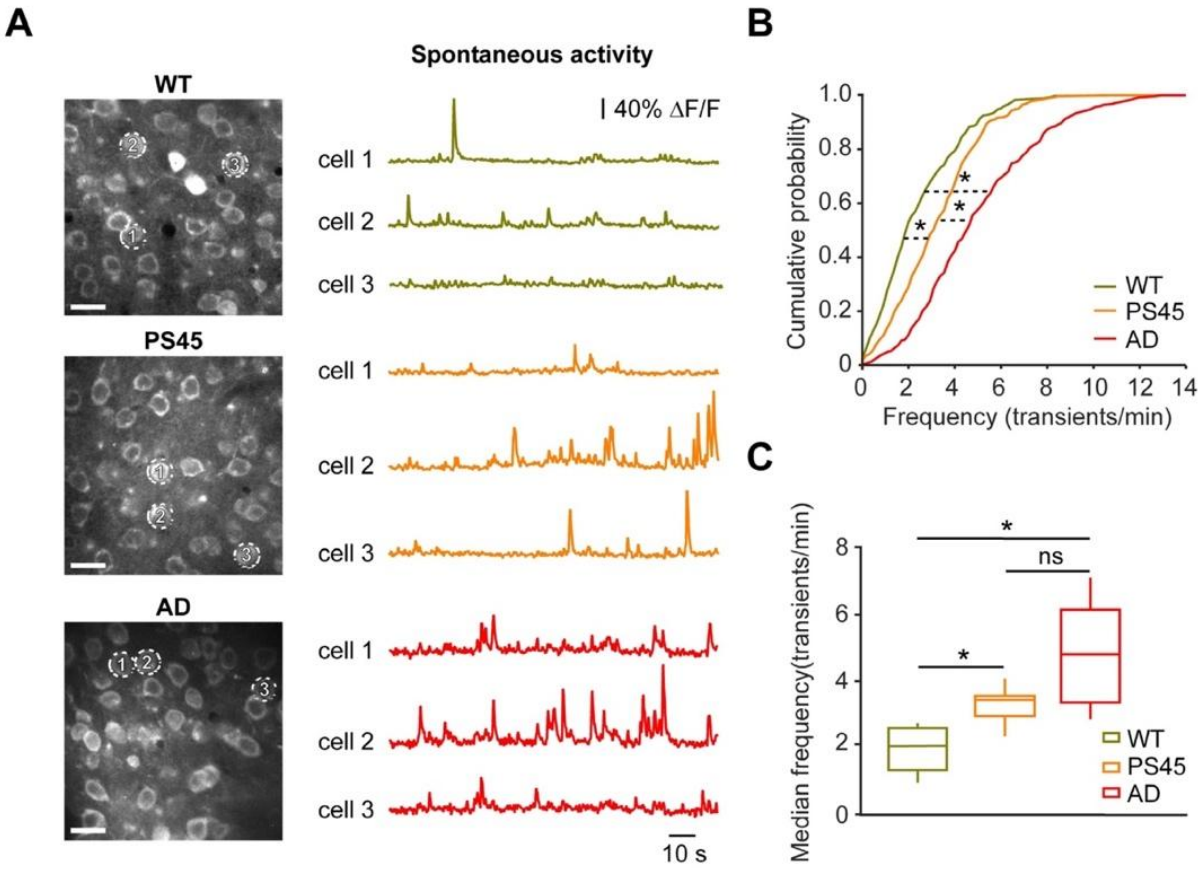


**Figure 15. Neuronal hyperactivity in the primary visual cortex of PS45 and AD mice. A** left, maximum MIP images of layer 2/3 neurons in a WT (top), a PS45 (middle) and an AD (bottom) mouse. Scale bars represent 10 µm. Right, spontaneous $Ca^{2+}$ transients recorded simultaneously from neurons marked with respective numbers in the corresponding left panel. **B**, cumulative probability functions showing frequency distributions of spontaneous $Ca^{2+}$ transients in WT (green), PS45 (orange) and AD (red) mice. The frequency distributions in PS45 and AD mice are significantly shifted towards higher frequencies compared to WT mice ($p < 0.01$ for all comparisons, Kolmogorov Smirnov test). **C**, box-and-whisker plot showing the median (per mouse) frequency of spontaneous $Ca^{2+}$ transients in WT (green), PS45 (orange) and AD (red) mice. The median frequencies in PS45 and AD mice are significantly higher compared to WT mice ($p = 0.03$ for WT vs. PS45, $p < 0.01$ for WT vs. AD and $p = 0.22$ for PS45 vs. AD, Kruskal-Wallis test). n = 7, 6, 6 mice for WT, PS45 and AD mice, respectively.

Altogether, these data documented the presence of neuronal hyperactivity in V1 of 10-12 months old $APP_{SWE}/PS1_{G384A}$ and even of 10-12 months old $PS1_{G384A}$ mice, presenting neither with plaque accumulation nor with neuroinflammation (Lerdkrai et al., 2018).

### 3.3 An impairment of visual response properties in mouse models of Alzheimer's disease

Next, we measured visually evoked neuronal response to the standard protocol (**Figure 4**) in layer 2/3 neurons in V1 of WT, PS45 and AD mice. **Figure 16** shows examples of three repeated trials as well as the corresponding averaged traces, recorded from representative visually responsive-neurons (marked with an arrowhead on a respective left panel) in WT (top), PS45 (middle) and AD (bottom) mice.

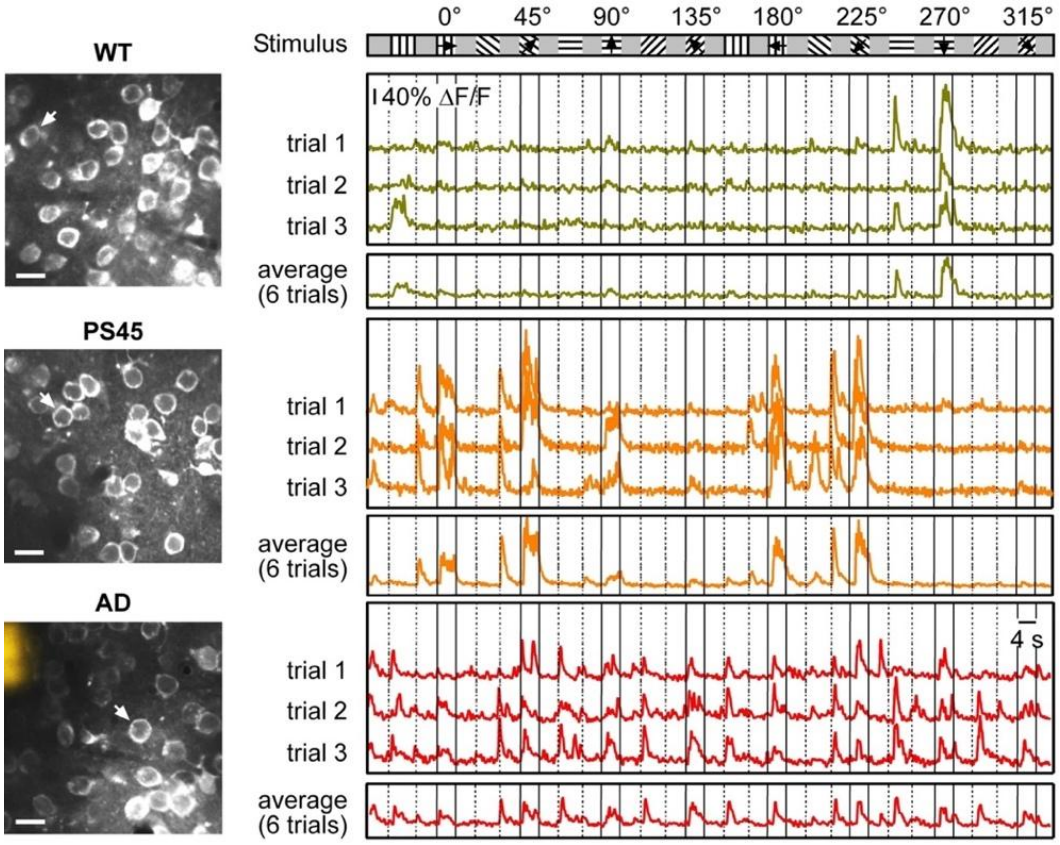


**Figure 16. Visual response properties in PS45 and AD mice.** Left, MIP images of layer 2/3 neurons in V1 of a WT (top), a PS45 (middle) and an AD (bottom) mouse. Right, three representative traces and an average of six trials recorded from neurons marked with an arrowhead in the corresponding left panel, in response to standard stimulation protocol (top row).

### 3.2.1 Pathologically increased visual responsiveness

Our visual stimulation protocol (**Figure 4**) was designed to enable analyses of neuronal responses to different kinds of visual stimuli, including drifting gratings, static gratings ON and static gratings OFF stimuli. In 10-12 months old WT mice, the fraction of layer 2/3 neurons responding to all kinds of visual stimuli was 57.3±13.3% (**Figure 17A**). Interestingly, in PS45 and AD mice the overall visual responsiveness was significantly higher, reaching 76.1±8.5% and 79.7±12.4%, respectively (**Figure 17A**). Moreover, compared to WT mice, both PS45 and AD mice showed a significant increase in visual responsiveness to drifting gratings stimuli (**Figure 17B**). In addition, in AD mice we observed a significantly increased fraction of neurons responding to static gratings ON (**Figure 17C**) and static gratings OFF (**Figure 17D**) stimuli. PS45 mice showed a similar trend but the observed difference did not reach the level of statistical significance (**Figure 17C, D**).

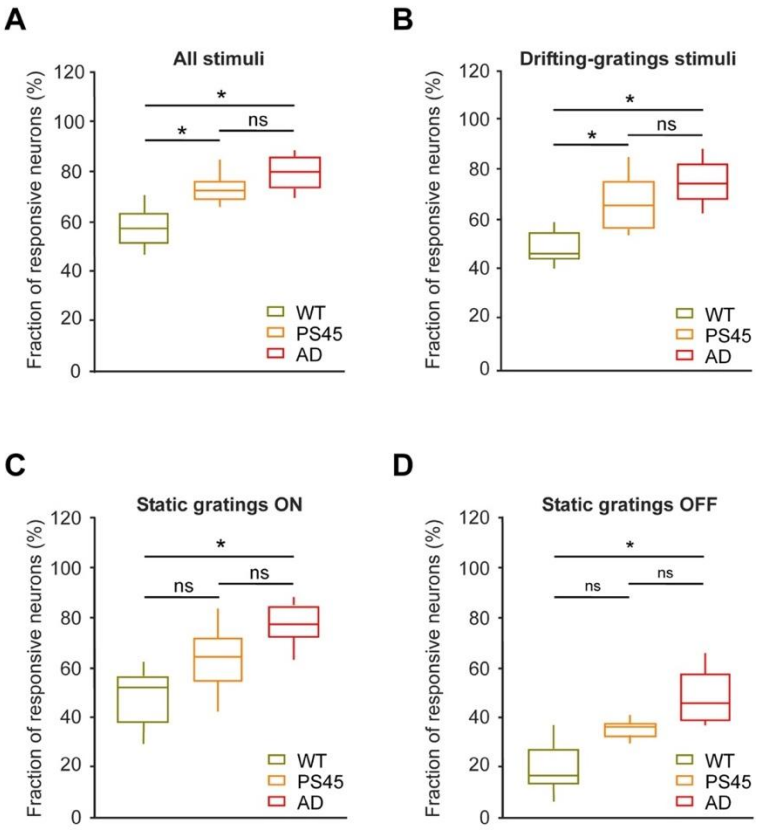


**Figure 17. Increased visual responsiveness in PS45 and AD mice**. **A-D**, box-and-whisker plots showing fractions (per mouse) of neurons responding to any visual stimulus (i.e. either drifting or static

ON/OFF gratings, **A**), drifting gratings (**B**), static gratings ON (**C**) and static gratings OFF (**D**) in WT (green), PS45 (orange) and AD (red) mice. In all cases fractions of responding neurons were significantly higher in AD compared to WT mice. (**A**: $p = 0.02$ for WT vs. PS45, $p < 0.01$ for WT vs. AD and $p = 0.28$ for PS45 vs. AD, Kruskal-Wallis test; **B**: $p = 0.03$ for WT vs. PS45, $p < 0.01$ for WT vs. AD and $p = 0.30$ for PS45 vs. AD , Kruskal-Wallis test; **C**: $p < 0.01$ for WT vs. AD, $p = 0.09$ for WT vs. PS45 and $p = 0.15$ for PS45 vs. AD, Kruskal-Wallis test; **D**: $p < 0.01$ for WT vs. AD, $p = 0.10$ for WT vs. PS45 and $p = 0.09$ for PS45 vs. AD, Kruskal-Wallis test). n = 7, 6, 6 mice for WT, PS45 and AD, respectively.

Due to an increase in spontaneous activity in AD mouse models, it can be possible that an increased visual responsiveness which is calculated from the average trial is caused by a contamination of spontaneous activity. Thus, an alternative method was used for defining visually responsive-neurons from the individual trials (for details see Materials and methods section). Similar results were obtained when individual trials were used to identify visually responsive-neurons. The fraction of neurons responding to all kinds of visual stimuli in PS45 and AD mice was significantly higher compared to WT mice ($p = 0.02$ for WT vs. PS45, $p = 0.01$ for WT vs. AD and $p = 0.88$ for PS45 vs. AD, Kruskal-Wallis Test; n = 7, 6, 6 for WT, PS45 and AD, respectively). In addition, the fractions of neurons responding to drifting gratings stimuli in PS45 and AD mice were also significantly higher compared to those encountered in WT mice ($p = 0.02$ for WT vs. PS45, $p = 0.03$ for WT vs. AD and $p = 0.90$ for PS45 vs. AD, Kruskal-Wallis Test; n = 7, 6, 6 for WT, PS45 and AD, respectively).

Taken together, these results showed an overall increase in visual responsiveness in 10-12 months old PS45 and AD mice. Interestingly, our data revealed a strong impairment of visual responsiveness in PS45 mice, despite the lack of plaque deposition and neuroinflammation in this mouse strain (Lerdkrai et al., 2018).

### 3.3.2 Increase in visually-evoked neuronal response to non-preferred stimuli

Further, the area under the curve of mean $Ca^{2+}$ transients evoked by the preferred and non-preferred directions (**Figure 18A, B**) as well as the preferred and non-preferred orientations (**Figure 18C, D**) of drifting gratings stimuli were calculated.

The visually responsive-neurons in PS45 and AD mice had higher AUCs of $Ca^{2+}$ transients evoked by the non-preferred directions and non-preferred orientations than visually responsive-neurons in WT mice (**Figure 18B, D**). However, the AUCs of $Ca^{2+}$ transients evoked by the preferred direction and orientation of drifting gratings stimuli in neurons of all three mouse strains were similar (**Figure 18A, C**).

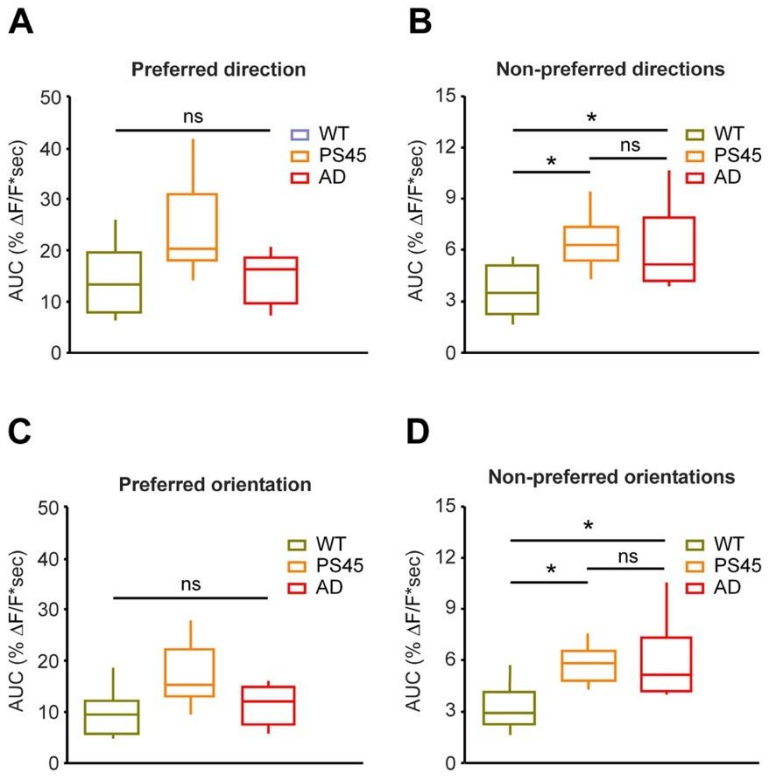


**Figure 18. Increased visually-evoked neuronal responses in PS45 and AD mice. A-D**, box-and-whisker plots showing the median (per mouse) areas under the curve (AUCs) of neuronal responses evoked by the preferred direction (**A**), non-preferred directions (**B**), preferred orientation (**C**) and non-preferred orientations (**D**) of drifting gratings stimuli in WT (dark green), PS45 (orange) and AD (red) mice. There was no significant difference in AUCs of neuronal responses evoked by the preferred direction and the preferred orientation in WT, PS45 and AD mice ((**A**) $p = 0.08$, (**C**) $p = 0.09$, Kruskal-Wallis test). AUCs of neuronal responses evoked by non-preferred directions and non-preferred orientations in PS45 and AD mice were significantly higher compared to WT mice ((**B**) $p < 0.01$, for WT vs. PS45, $p < 0.05$, for WT vs. AD and $p = 0.44$ for PS45 vs. AD, Kruskal-Wallis test; (**D**) $p < 0.01$, for WT vs. PS45, $p = 0.04$ for WT vs. AD and $p = 0.57$ for PS45 vs. AD, Kruskal-Wallis test).

### 3.3.3 Visual tuning properties are differentially affected in $PS1_{G384A}$ and $APP_{swe}/PS1_{G384A}$

To test whether visual tuning properties are changed in PS45 and AD mice, we compared DSI (**Figure 19A**) and OSI (**Figure 19B**) of visually responsive-neurons in WT, PS45 and AD mice. The DSI of visually responsive-neurons in PS45 and AD mice showed similar distributions on a population level, and the DSI distributions in both mouse strains were significantly shifted to lower values, compared to the DSI distribution in WT mice (**Figure 19A, left**). When comparing AD and WT mice, a similar finding was observed when analyzing the distribution of the median DSI values per mouse (**Figure 19A, right**). The median DSI value in PS45 mice was also lower compared to that found in WT mice. This difference, however, did not reach the level of statistical significance. Furthermore, visually responsive-neurons in AD mice had a significantly lower OSI, when compared with visually responsive-neurons in WT mice. Interestingly, the visually responsive-neurons in PS45 mice, despite exhibiting a decrease in the direction tuning (**Figure 19A**), had an orientation tuning similar to that of visually responsive-neurons in WT mice (**Figure 19B**).

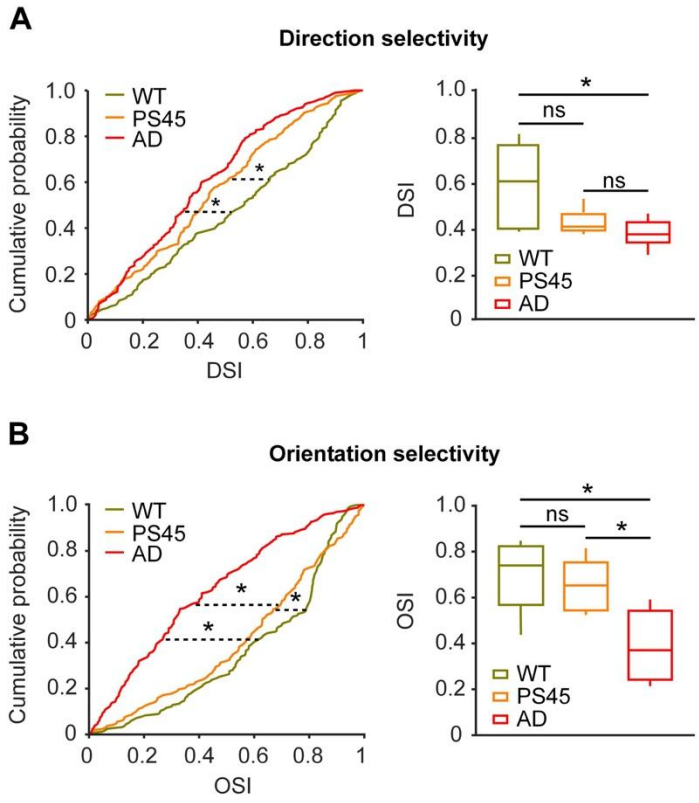


**Figure 19. Visual tuning properties are differentially affected in PS45 and AD mice. A, B** (left), cumulative probability functions showing the distributions of DSI (**A**) and OSI (**B**) of neurons in WT (dark green), PS45 (orange) and AD (red) mice. Neurons in PS45 and AD mice had lower DSI compared to WT mice ($p < 0.01$ for both comparisons and $p = 0.08$ for PS45 vs. AD, Kolmogorov Smirnov test). Neurons in AD mice had lower OSI compared to WT and PS45 mice; neurons in PS45 mice had lower OSI compared to WT mice ($p < 0.01$ for all comparisons, Kolmogorov Smirnov test). **A, B** (right), box-and-whisker plots showing the median (per mouse) DSI (**A**) and OSI (**B**) in WT (dark green), PS45 (orange) and AD (red) mice. The median DSI in AD mice was lower compared to WT mice ($p < 0.01$ for WT vs. AD, $p = 0.11$ for WT vs. PS45 and $p = 0.33$ for PS45 vs. AD, Kruskal-Wallis test), and the median OSI in AD mice was lower compared to WT and PS45 mice ($p < 0.01$ for WT vs. AD, $p = 0.03$ for PS45 vs. AD and $p = 0.66$ for WT vs. PS45, Kruskal-Wallis test).

The visually responsive-neurons in AD mice (**Figure 20C**, right) also showed a wider response function to oriented drifting gratings than visually responsive-neurons in WT (**Figure 20C**, left) and PS45 (**Figure 20C**, middle) mice. To compare the response functions to oriented drifting gratings, the circular variance for all responses of each individual neuron was calculated. Visually responsive-neurons from AD mice had significantly higher circular variances compared to those found in WT mice, whereas

circular variances of visually responsive-neurons in PS45 mice had intermediate values (**Figure 20D**).

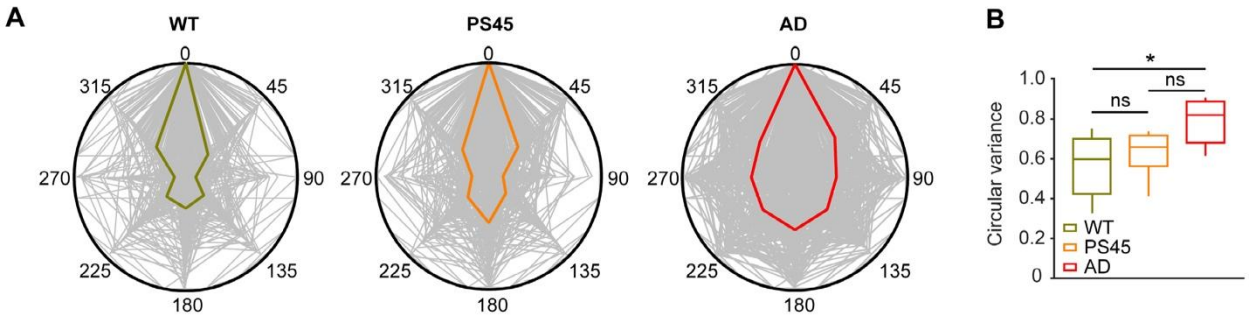


**Figure 20. Circular variance is increased in AD mice. A**, polar plots showing response functions of all neurons (grey) to oriented drifting gratings in WT, PS45 and AD mice. The medians of neuronal responses in WT, PS45 and AD mice are shown as dark green, orange and red lines, respectively. **B**, box-and-whisker plot showing the median (per mouse) circular variance in WT (dark green), PS45 (orange) and AD (red) mice. Circular variance increased in AD mice, compared to WT mice ($p = 0.01$ for WT vs. AD, $p = 0.56$ for WT vs. PS45 and $p = 0.07$ for PS45 vs. AD, Kruskal-Wallis test). WT: n = 156 neurons, 7 mice; PS45: n = 163 neurons, 6 mice; AD: n = 203 neurons, 6 mice.

Taken together, these data revealed a profound impairment of tuning properties in AD mice. The latter included a significant decrease in DSI as well as OSI and a significant increase in the circular variance. When considering the direction selectivity, the tuning properties of PS45 mice were similar to that of AD mice, but when considering orientation selectivity and the circular variance, they were more similar to that of WT mice.

### 3.3.4 Visual tuning properties are impaired in both normal and hyperactive neurons

In the AD mouse strain used in this study, the impairment of the orientation selectivity was previously reported to occur selectively in hyperactive neurons (Grienberger et al 2012). Therefore, next we analyzed the correlation between the frequency of spontaneous activity in individual neurons and their visual tuning

properties. To do so, the frequency of spontaneous $Ca^{2+}$ transients of a respective neuron was measured first during the presentation of a dark screen. Thereafter, we run our usual stimulation protocol (**Figure 4**), to determine the neuron's DSI, OSI and the circular variance.

For a direct comparison with the previous study, all recorded neurons were classified as silent, normal and hyperactive based on the frequency of their ongoing spontaneous $Ca^{2+}$ transients (the frequency ranges are given in the materials and methods section, the same analyses as in (Busche et al., 2008; Grienberger et al., 2012; Lerdkrai et al., 2018) and the tuning properties of normal and hyperactive neurons were compared in the three mouse strains. In contrast to what was found in younger AD mice, in which the AD-related impairment was restricted to the hyperactive cells only (Grienberger et al 2012), both normal and hyperactive cells showed an impairment of visual tuning properties in 10-12 months old PS45 and AD mice (**Figure 21**), virtually repeating findings presented in **Figure 19A, B** for the entire neuronal population.

These results revealed a progression of AD-related visual impairment in 10-12 months old mice to the whole neuronal population

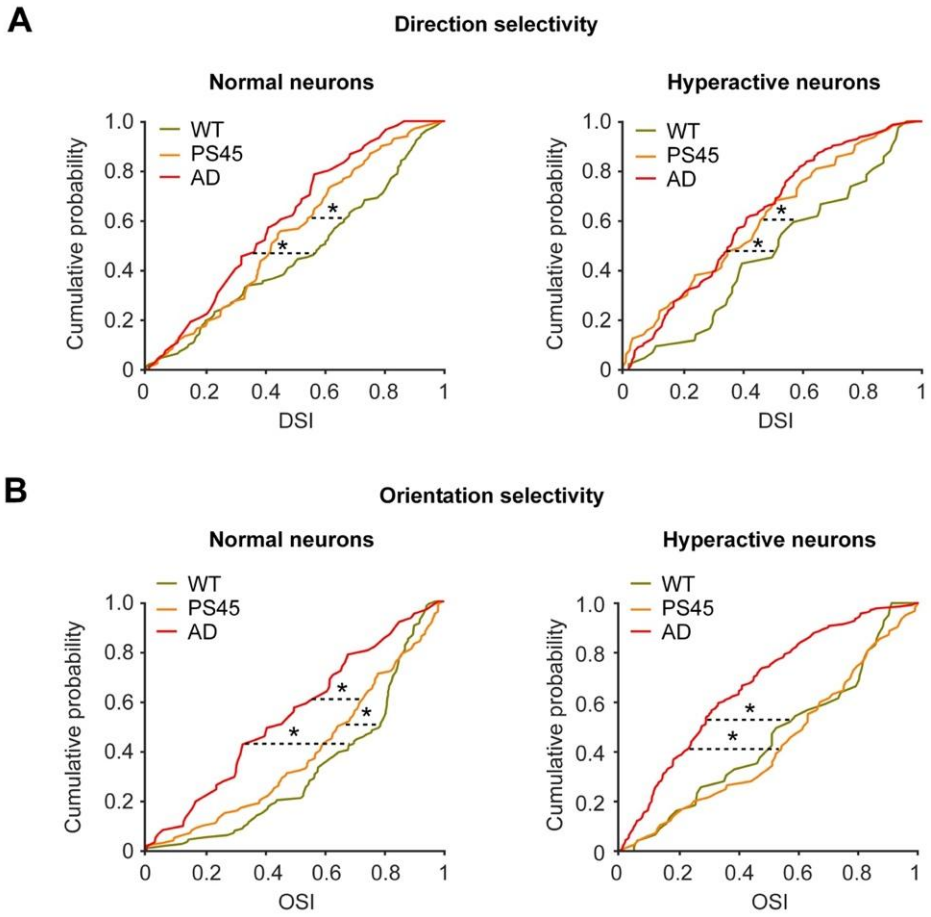


**Figure 21. Visual tuning properties are impaired in both normal and hyperactive neurons. A, B**, cumulative probability functions showing the distributions of DSI of normal (**A**, left) and hyperactive (**A**, right) neurons and OSI of normal (**B**, left) and hyperactive (**B**, right) neurons in WT (dark green), PS45 (orange) and AD (red) mice. In normal and hyperactive neurons of PS45 and AD mice the distributions of DSI are significantly shifted towards the lower values compared to respective distributions recorded in WT mice (**A**, left: $p = 0.03$ for WT vs. PS45, $p < 0.01$ for WT vs. AD and $p = 0.16$ for PS45 vs. AD, Kolmogorov Smirnov test; **A**, right: $p = 0.04$ for WT vs. PS45, $p = 0.01$ for WT vs. AD and $p = 0.60$ for PS45 vs. AD, Kolmogorov Smirnov test). The distributions of OSI of normal and hyperactive neurons recorded in AD mice are significantly shifted towards the lower values compared to WT and PS45 mice and the distribution of OSI in normal neurons of PS45 mice is slightly but significantly shifted towards lower OSI compared to the respective distribution recorded in WT mice (**B**, left: $p < 0.01$ for all comparisons, Kolmogorov Smirnov test; **B**, right: $p = 0.65$ for WT vs. PS45, $p < 0.01$ for WT vs. AD, $p < 0.01$ for PS45 vs. AD, Kolmogorov Smirnov test). Normal neurons, WT: n = 110 neurons, 7 mice; PS45: n = 99 neurons, 6 mice; AD: n = 61 neurons, 6 mice; Hyperactive neurons, WT: n = 42 neurons, 7 mice; PS45: n = 63 neurons, 6 mice; AD: n = 142 neurons, 6 mice.

### 3.3.5 The degree of visual impairment correlated with the degree of neuronal hyperactivity

Next we studied the relationship between neuronal hyperactivity and visual tuning properties. To do so, correlations between the frequencies of spontaneous $Ca^{2+}$ transients and the visual tuning properties (DSI, OSI and circular variance) of a neuron were calculated by GEE. There was no correlation between DSI and the frequency of spontaneous $Ca^{2+}$ transients in visually responsive-neurons of all WT, PS45 and AD mice (**Figure 22A-C**). However, there was a significant correlation between OSI and the frequency of spontaneous $Ca^{2+}$ transients in visually responsive-neurons in all three mouse strains (**Figure 22D-F**). Similar to OSI, circular variance of neuronal responses in WT (**Figure 22G**) and AD (**Figure 2I**) mice was significantly correlated with the frequency of spontaneous $Ca^{2+}$ transients in these neurons. In neurons from PS45 mice (**Figure 22H**) there also was a trend towards such a correlation. However, the correlation coefficient in this case did not reach the level of statistical significance.

Altogether, these data document the presence of neuronal hyperactivity in the visual cortex of both PS45 and AD mouse strains and reveal a linear relationship between the frequency of ongoing neuronal activity and the degree of impairment of their orientation selectivity and, to a lesser extent, the circular variance of their visual responses on a single cell level.

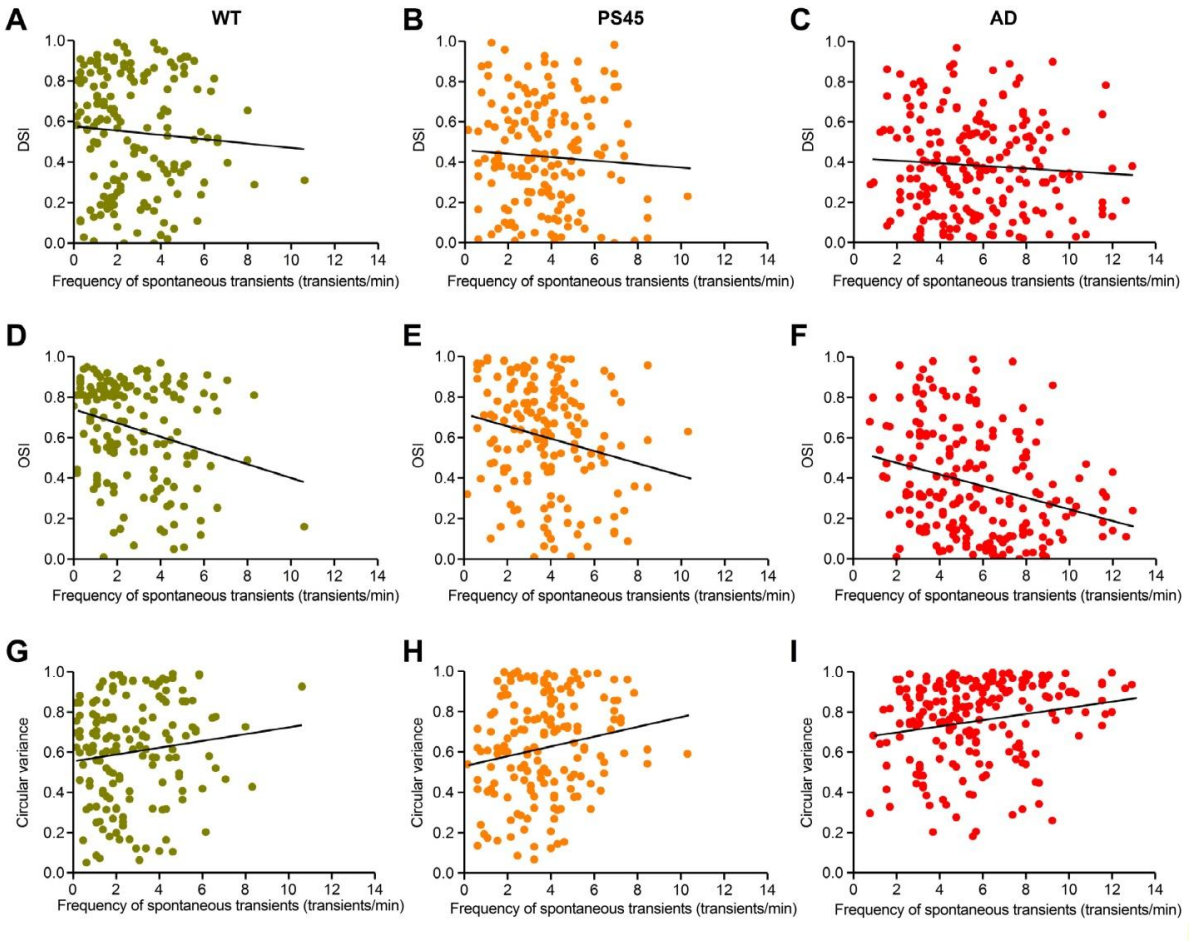


**Figure 22. The degree of visual impairment correlates with the degree of neuronal hyperactivity. A-C**, scatter plots illustrating the relationship between the frequency of spontaneous $Ca^{2+}$ transients and DSI of all visually responsive-neurons in WT (**A**), PS45 (**B**) and AD (**C**) mice. There is no correlation between the frequency of spontaneous $Ca^{2+}$ transients and DSI in all mouse lines tested ($p = 0.91$, $R = 0.04$ for WT, $p = 0.20$, $R = -0.06$ for PS45 and $p = 0.63$, $R = -0.07$ for AD mice, GEE). **D-F**, scatter plots illustrating the relationship between the frequency of spontaneous $Ca^{2+}$ transients and OSI of all visually responsive-neurons in WT (**D**), PS45 (**E**) and AD (**F**) mice. Visually responsive-neurons in all mouse lines show negative correlation between the frequency of spontaneous $Ca^{2+}$ transients and OSI ($p < 0.01$, $R = -0.27$ for WT, $p < 0.01$, $R = -0.22$ for PS45 and $p = 0.03$, $R = -0.29$ for AD mice, GEE). **G-I**, scatter plots illustrating the relationship between the frequency of spontaneous $Ca^{2+}$ transients and the circular variance of all visually responsive-neurons in WT (**G**), PS45 (**H**) and AD (**I**) mice. Visually responsive-neurons in WT and AD mice show a positive correlation between the frequency of spontaneous $Ca^{2+}$ transients and the circular variance ($p < 0.01$, $R = 0.13$ for WT, $p = 0.06$, $R = 0.19$ for PS45 and $p = 0.03$, $R = 0.20$ for AD mice, GEE). WT: n = 156 neurons, 7 mice; PS45: n = 163 neurons, 6 mice; AD: n = 203 neurons, 6 mice. Data were analyzed by Prof. Dr. Peter Martus.

### 3.3.6 Impairment of the stimulus-induced suppression of spontaneous activity in $APP_{swe}/PS1_{G384A}$

When conducting the imaging protocol described above (**Figure 4**), we noticed that in WT mice spontaneous $Ca^{2+}$ transients, abundant during the presentation of a dark screen, almost disappeared during the visual stimulation (**compare Figure 15A with Figure 16**). Hence, we measured the frequency of spontaneous $Ca^{2+}$ transients during the intermittent resting periods while presenting visual stimuli (grey screen presentation, see **Figure 16**) and compared it with the frequency of spontaneous $Ca^{2+}$ transients measured in the same neuron before the presentation of the visual stimuli (dark screen presentation, as in **Figure 15A**). The analyses of these data (**Figure 23**) revealed a clear suppression of spontaneous activity by visual stimuli in visually responsive-neurons of WT (**Figure 23A**), and PS45 (**Figure 23B**) mice. In AD mice, however, the suppression was much less prominent (**Figure 23C**). To quantify these observations, we calculated the ratio between the frequencies of $Ca^{2+}$ transients recorded before and during the presentation of the visual stimuli (Activity ratio). In WT mice (**Figure 23D**), the median (per mouse) activity ratio was 0.49 ± 0.32, documenting a clear suppression of spontaneous activity by visual stimuli. The neurons in PS45 mice showed a similar median activity ratio (0.47 ± 0.16), whereas the median activity ratio in AD mice (0.71 ± 0.27) was significantly higher, documenting a clear lack of suppression of spontaneous activity by visual stimuli in this mouse strain (**Figure 23D**).

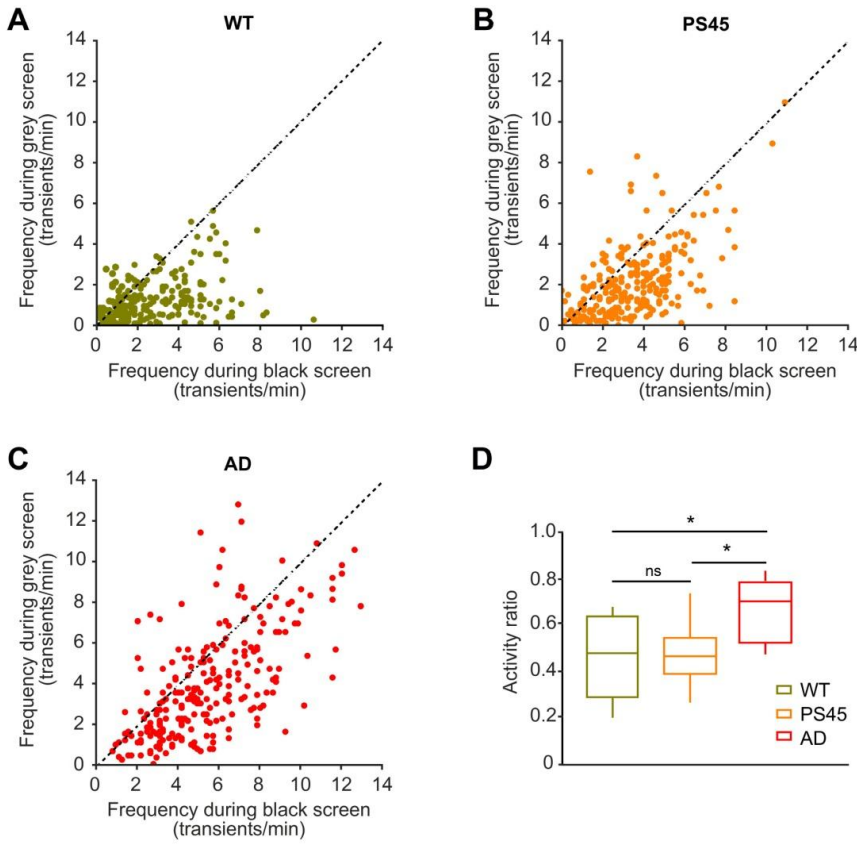


**Figure 23. Impairment of the stimulus-induced suppression of spontaneous activity in AD mice. A-C**, scatter plots illustrating the relationship between the frequency of spontaneous transients during the presentation of the black screen (X-axis) and the grey screen (Y-axis) for all visually responsive-neurons in WT (**A**), PS45 (**B**) and AD (**C**) mice. **D**, box-and-whisker plot showing the median (per mouse) activity ratios for all visually responsive-neurons of WT (dark green), PS45 (orange) and AD (red) mice. The stimulation-induced suppression of spontaneous $Ca^{2+}$ transients is significantly impaired in AD compared to WT and PS45 mice ($p = 0.04$ for WT vs. AD, $p = 0.02$ for PS45 vs. AD and $p = 0.72$ for WT vs. PS45, Kruskal-Wallis test). n = 7, 6, 6 mice for WT, PS45 and AD, respectively.

Taken together, these data reveal that visually responsive-neurons in WT and PS45 mice exhibit a strong sensory stimulus-induced suppression of the spontaneous activity and that this suppression is impaired in AD mice.

## 3.4 The effect of depletion of the intracellular $Ca^{2+}$ stores by a SERCA blocker

Because the impairment of the orientation selectivity and the circular variance of visual responses turned out to be correlated with the degree of neuronal hyperactivity and the intracellular $Ca^{2+}$ stores have an important role for controlling neuronal hyperactivity in mouse models of AD (Lerdkrai et al., 2018), we studied whether depleting the stores could rescue the impairment of visual processing.

### 3.4.1 Store depletion reduces neuronal hyperactivity in V1 of both $PS1_{G384A}$ and $APP_{swe}/PS1_{G384A}$

First, the effect of CPA on the neuronal hyperactivity in V1 of WT, PS45 and AD mice was tested. To do so, the frequency of spontaneous $Ca^{2+}$ transients of layer 2/3 neurons was recorded before and during the application of 400 µM CPA (30-min-long pretreatment; this protocol completely abolishes caffeine-induced $Ca^{2+}$ release from the intracellular $Ca^{2+}$ stores in layer 2/3 neurons *in vivo* see Materials and methods section). CPA application reduced the fraction of hyperactive neurons in AD mice from 58% to 37% and increased the fraction of normal neurons from 40% to 60% (Figure **24A**). A similar effect was also observed in PS45 mice. At the level of the entire population CPA significantly reduced the frequency of spontaneous $Ca^{2+}$ transients in PS45 and AD mice, without affecting the frequency of spontaneous $Ca^{2+}$ transients in WT mice (**Figure 24B-E**).

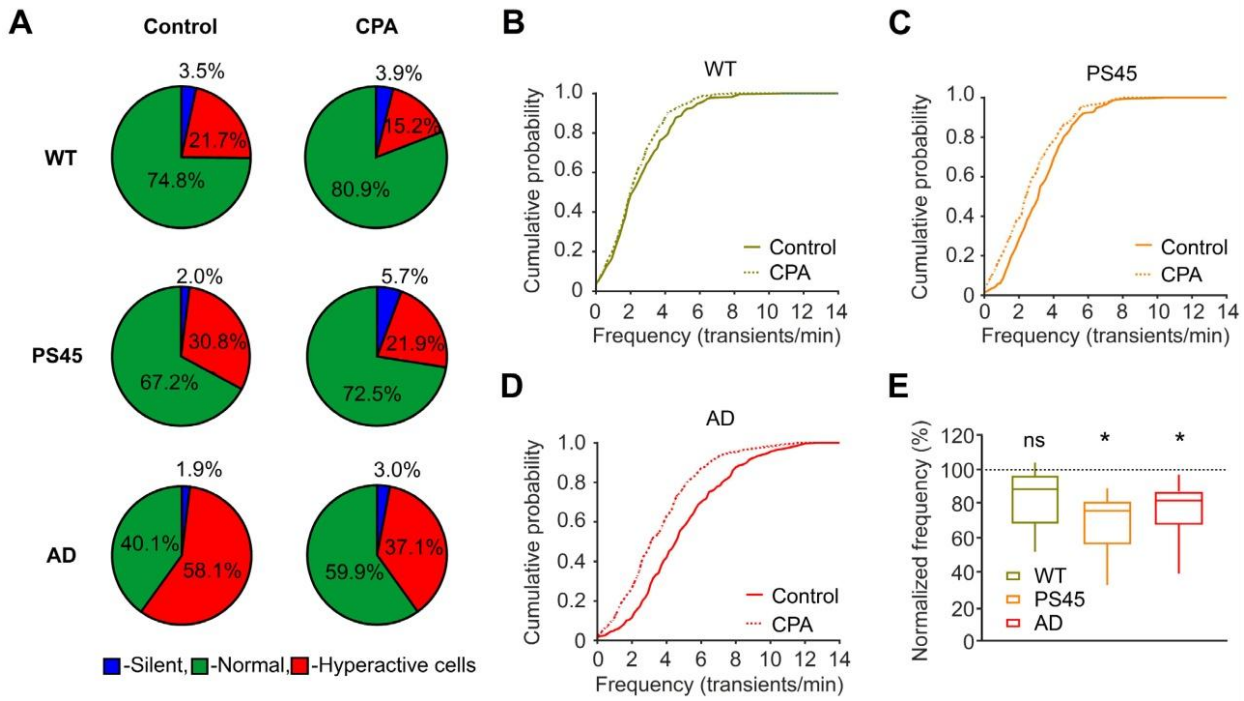


**Figure 24 Store depletion reduced neuronal hyperactivity in both PS45 and AD mice. A**, pie charts illustrating the fractions of silent (blue), normal (green) and hyperactive (red) neurons before (Control) and during the application of CPA (CPA) in WT (top), PS45 (middle) and AD (bottom) mice. **B-D**, cumulative probability functions showing the frequency distributions of spontaneous $Ca^{2+}$ transients before (Control) and during the application of CPA (CPA) in WT (**B**), PS45 (**C**) and AD (**D**) mice. **E**, box-and-whisker plot showing the effect of CPA on the frequency of spontaneous $Ca^{2+}$ transients in WT (dark green), PS45 (orange) and AD (red) mice. Data are shown as median (per mouse) values under CPA normalized to the respective control values. The frequency of spontaneous $Ca^{2+}$ transients significantly decreased under CPA in PS45 and AD mice ($p < 0.01$ for PS45, $p = 0.01$ for AD and $p = 0.08$ for WT, two-way rANOVA). n = 5, 6, 6 mice for WT, PS45 and AD, respectively.

These data show that neuronal hyperactivity in V1 of PS45 and AD mice is also caused by dysfunction of intracellular $Ca^{2+}$ stores and document the ability of CPA to reduce the AD-mediated neuronal hyperactivity in this brain area.

### 3.4.2 Store depletion ameliorates the pathological increase in visual responsiveness

In the next series of experiments, we tested whether reducing neuronal hyperactivity by store depletion in PS45 and AD mice can counteract the impairment of visual response properties. First, we tested whether the presence of CPA changes the fraction of visually responsive-neurons, which is increased in PS45 and AD mice (**Figure 17**). As shown in **Figure 25**, CPA significantly reduced pathologically increased visual responsiveness to all visual stimuli and to drifting gratings stimuli both in PS45 and AD mice, without changing visual responsiveness in WT mice. Actually, under CPA the fractions of visually responsive-neurons in PS45 and AD mice were not significantly different from those in WT mice under control conditions ($p = 0.34$ for all visual stimuli and $p = 0.36$ for drifting gratings stimuli, Kruskal-Wallis test; n = 5, 6, 6 mice for WT, PS45 and AD, respectively). Similar results were obtained when analyzing only neurons identified as visually responsive based on individual trials (all visual stimuli: $p = 0.63$ for WT, $p = 0.03$ for PS45 and $p = 0.03$ for AD; drifting gratings stimuli: $p = 0.99$ for WT, $p = 0.03$ for PS45 and $p = 0.03$ for AD, Wilcoxon Signed-Rank test;. n = 5, 6, 6 mice for WT, PS45 and AD, respectively).

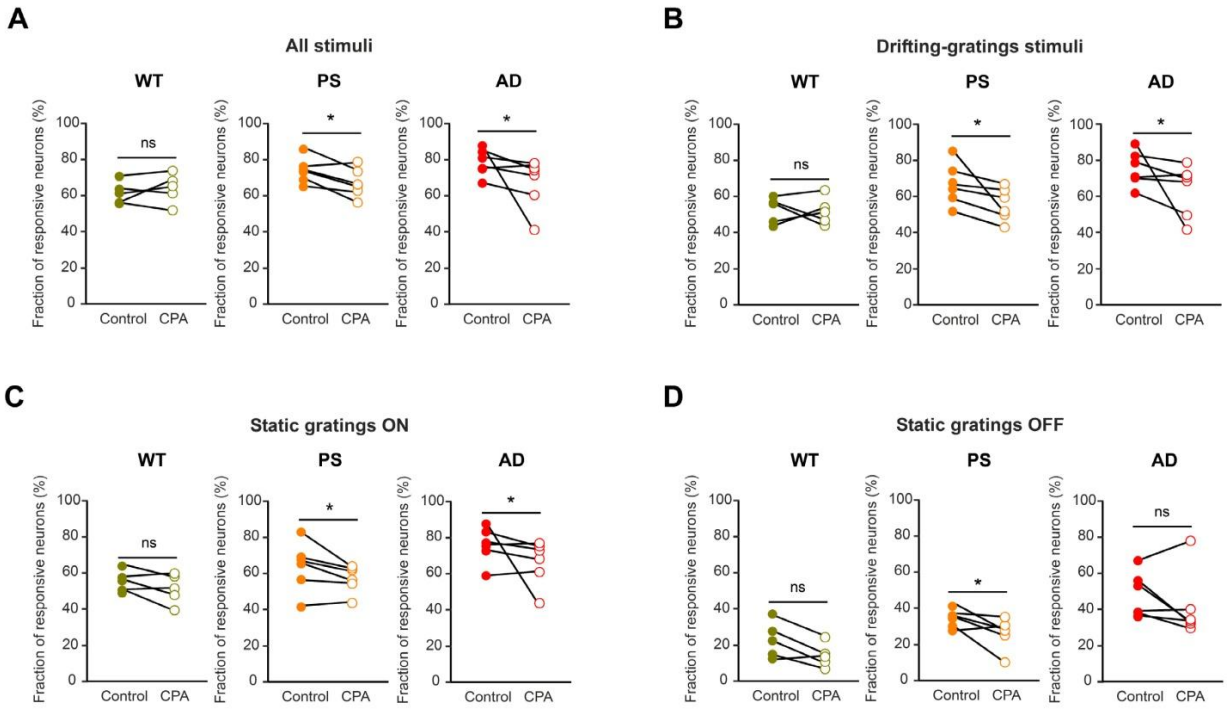

**Figure 25. Store depletion ameliorates the pathological increase in visual responsiveness. A-D**, dot plots showing the effect of CPA-mediated store blockade on the fractions of visually responsive-neurons in WT (dark green), PS45 (orange) and AD (red) mice. ((**A**) p = 0.41 for WT, p = 0.046 for PS45 and p = 0.03 for AD, Wilcoxon Signed-Rank test; (**B**) p = 0.41 for WT, p = 0.02 for PS45 and p = 0.03 for AD, Wilcoxon Signed-Rank test; (**C**) p = 0.16 for WT, p = 0.03 for PS45 and p = 0.046 for AD, Wilcoxon Signed-Rank test; (**D**) p = 0.06 for WT, p = 0.03 for PS45 and p = 0.16 for AD, Wilcoxon Signed-Rank test;). n = 5, 6, 6 mice for WT, PS45 and AD, respectively.

Further, we tested whether CPA can recover the sensory stimulus-induced suppression of spontaneous activity (**Figure 23**) in AD mice. However, the activity ratios before and during CPA application in WT, PS45 and AD mice remained the same (**Figure 26**).

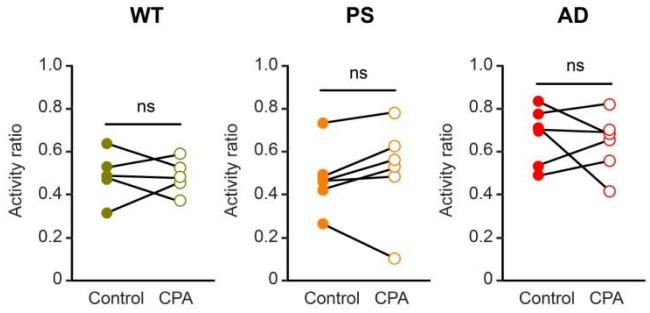


**Figure 26. CPA has no effect on the activity ratios.** Dot plots showing the effect of CPA-mediated store blockade on activity ratio in WT (dark green), PS45 (orange) and AD (red) mice (p = 0.5 for WT, p = 0.22 for PS45 and p = 0.42 for AD mice, Wilcoxon-Signed-Rank test). n = 5, 6, 6 mice for WT, PS45 and AD, respectively.

### 3.4.3 CPA-mediated store depletion does not improve visual tuning properties

Next, we analyzed the visual tuning properties before and during the application of CPA. Polar plots (**Figure 27**) illustrate the effect of CPA on neuronal responses to oriented drifting gratings in WT (left), PS45 (middle) and AD (right) mice.

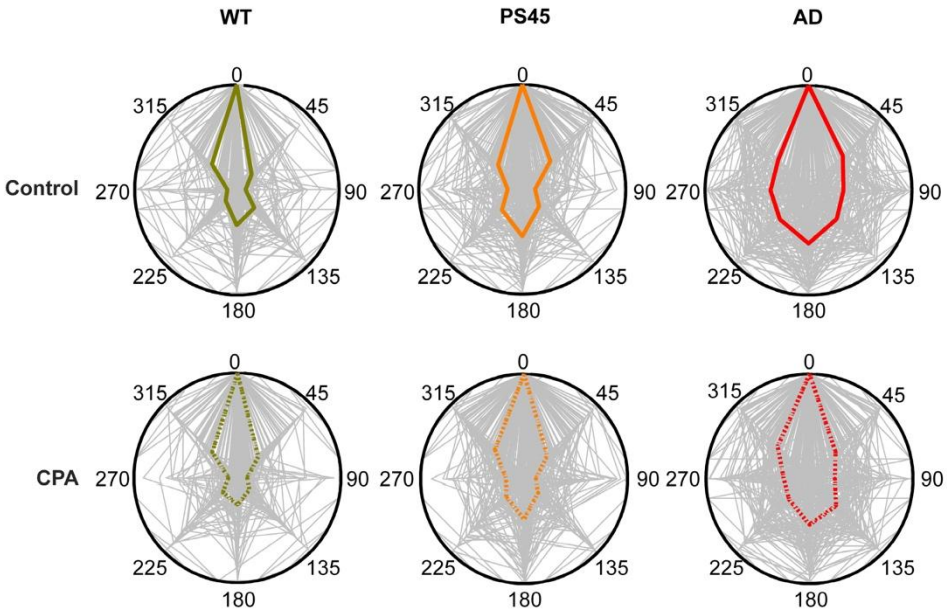


**Figure 27. Effect of the CPA-mediated store depletion on the response functions to oriented drifting gratings. A**, polar plots showing response functions (grey) to oriented drifting gratings of all visually responsive-neurons before (upper) and during (lower) application of CPA in WT (left), PS45 (middle) and AD (right) mice. The medians of neuronal responses in Control (solid line) and under CPA (dashed line) in WT, PS45 and AD mice are shown as dark green, orange and red lines, respectively.

Unexpectedly, the reduction of neuronal hyperactivity by CPA in PS45 and AD mice had no effect on the DSI, OSI and circular variance of neuronal responses both on a single cell level (**Figure 28**) and when analyzing the median effect per mouse (**Figure 29**).

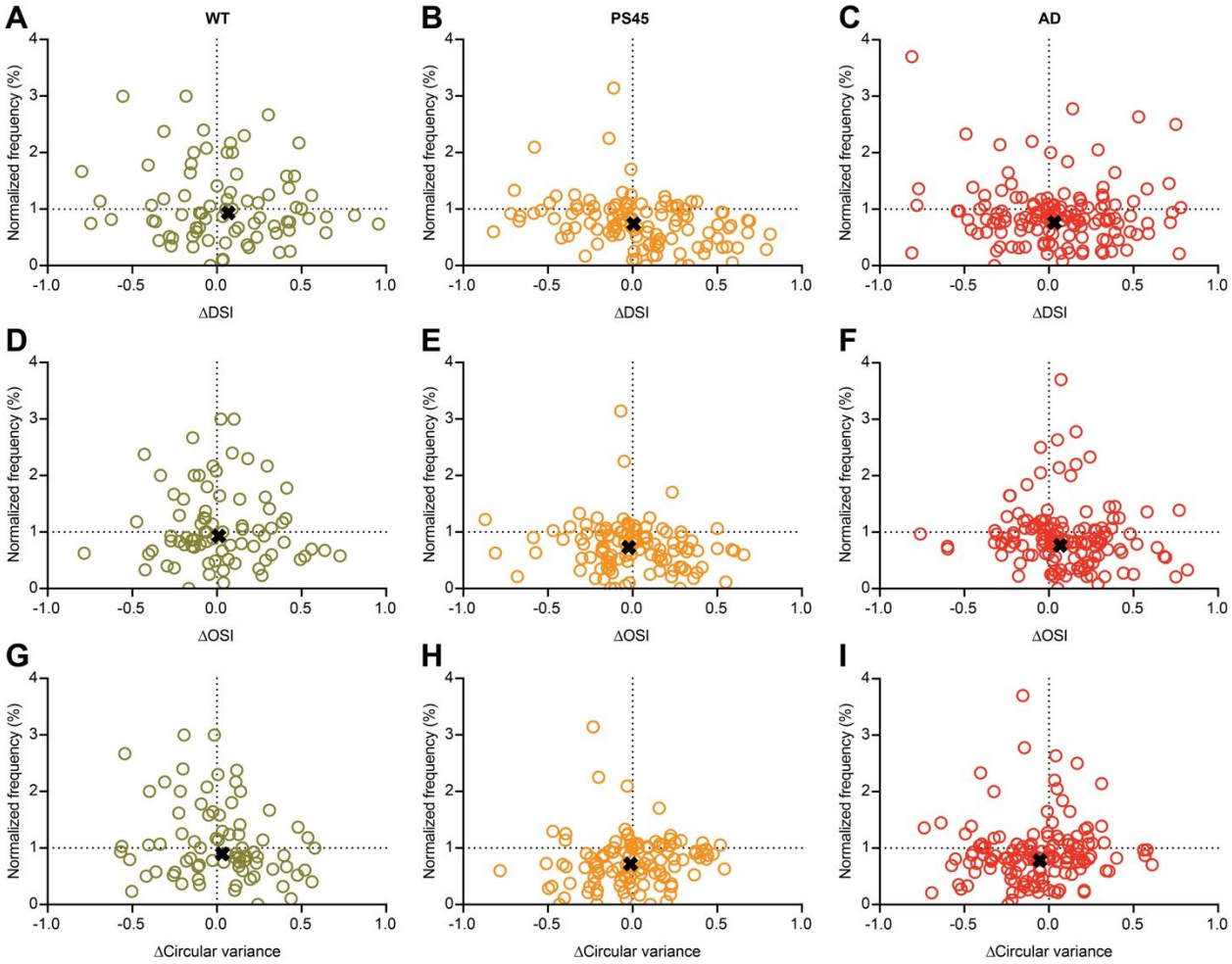


**Figure 28. The impaired orientation/direction tuning in PS45 and AD mice could not be rescued by CPA. A-C**, scatter plots illustrating the relationship between the effect of CPA on DSI (ΔDSI = DSI during CPA – DSI before CPA) and the effect of CPA on the frequency of spontaneous $Ca^{2+}$ transients (Normalized frequency = frequency during CPA / frequency before CPA) of all visually responsive-neurons in WT (**A**), PS45 (**B**) and AD (**C**) mice. **D-F**, scatter plots illustrating the relationship between the effect of CPA on OSI (ΔOSI = OSI during CPA – OSI before CPA) and on the frequency of spontaneous $Ca^{2+}$ transients (Normalized frequency) of all visually responsive-neurons in WT (**D**), PS45 (**E**) and AD (**F**) mice. **G-I**, scatter plots illustrating the relationship between the effect of CPA on the circular variance (Δcircular variance = circular variance during CPA – circular variance before CPA) and on the frequency of spontaneous $Ca^{2+}$ transients (Normalized frequency) of all visually responsive-neurons in WT (**G**), PS45 (**H**) and AD (**I**) mice. Cross marks are representing the median effect of CPA. WT: n = 80 neurons, 5 mice; PS45: n = 112 neurons, 6 mice; AD n = 140 neurons, 6 mice.

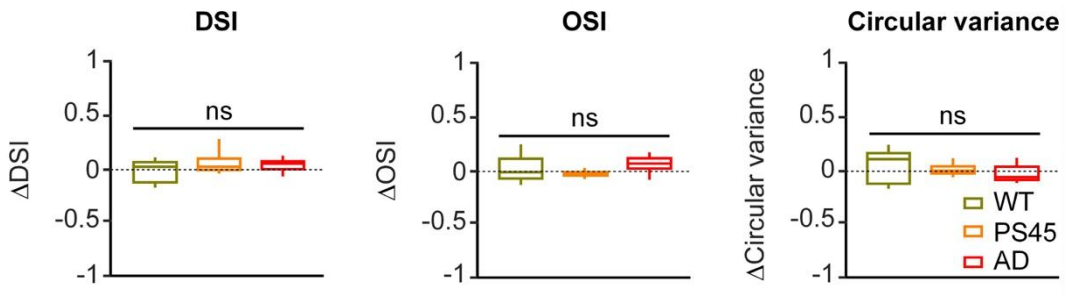


**Figure 29. CPA-mediated store depletion does not improve visual tuning properties.** Box-and-whisker plots showing the effect of CPA on the DSI, OSI and circular variance in WT (dark green), PS45 (orange) and AD (red) mice. Data are shown as the median (per mouse) ΔDSI (DSI during CPA – DSI before CPA, top), ΔOSI (OSI during CPA – OSI before CPA, middle) and Δcircular variance (circular variance during CPA – circular variance before CPA, bottom). CPA had no effect on the DSI, OSI and circular variance in all mouse strains ($p = 0.54$ for ΔDSI, $p = 0.23$ for ΔOSI and $p = 0.89$ for Δcircular variance, two-way rANOVA). n = 5, 6, 6 mice for WT, PS45 and AD, respectively.

In summary, these data suggest that $Ca^{2+}$ store-mediated neuronal hyperactivity contributes to a pathological increase of visual responsiveness in PS45 and AD mice. The latter can thus be ameliorated by emptying of the intracellular stores by CPA. At the same time, the stimulus-induced suppression of the spontaneous activity, as well as the impairment of visual tuning properties likely relies on different cellular/molecular mechanisms, which remain to be elucidated.

# 4 Discussion

## 4.1 Different development of neuronal hyperactivity among brain regions during ageing

This study shows that the age-related increase in neuronal hyperactivity indeed occurs in V1. Interestingly, it further reveals a different age-related progression of neuronal hyperactivity, when compared to other brain regions. Specifically, our previous study showed that the development of neuronal hyperactivity in the frontal/motor cortex occurs at the age of 10-14 months, which is rather early, before the animals are even considered aged (Flurkey K et al., 2007), and the neuronal hyperactivity remains high till the age of 18 months. In contrast, this study shows that age-related neuronal hyperactivity in V1 develops later, at the age of 18 months. This difference in development of neuronal hyperactivity provides the evidence for a higher vulnerability of the frontal/motor cortex to ageing compared to V1. These data are consistent with the progression pattern of age-related neurodegenerative diseases, such as Alzheimer's disease (Jucker and Walker, 2013).

The reason for this pronounced difference in the progression of age-related neuronal hyperactivity throughout the brain still remains unclear. One possible explanation comes from the study of lipid peroxidation during ageing in several brain regions of the post mortem human brain (Dominguez-Gonzalez et al., 2018; Naudi et al., 2017). Interestingly, Naudi et al show that when compared to other cortical areas, the frontal cortex is the most susceptible area to peroxidative damage (Naudi et al., 2017). An increase in the lipid peroxidation is well-known as one of the key functional changes during ageing (Mattson and Magnus, 2006) and this might lead to earlier development of age-related neuronal hyperactivity in frontal cortex compared to visual cortex.

## 4.2 Ageing related functional changes of neuronal properties in V1

Besides the development of neuronal hyperactivity during ageing, ageing also relates with a decrease in orientation tuning of visual response properties. Fascinatingly, this age-related change in visual response properties also develops at

later age. When compared with 3 or 10-12 months old mice, the 18 months old WT mice exhibit a decrease in orientation tuning without any change in the visual responsiveness, direction tuning properties or circular variance. This finding provided a direct evidence for the relationship between age-related neuronal hyperactivity and other functional impairments by showing that in V1 the age-related impairment of orientation tuning properties occurs at the same time (18 months old of age) as the onset of the age-related neuronal hyperactivity. In addition, our statistical analysis showed the positive correlation between the level of neuronal activity and the impairment of orientation selectivity. Taken together, these results provided a complete picture of the ageing-related changes in V1 during 3 different phases of life (young adult, middle-age and aged mice). This finding is supported by several studies about the normal ageing of human and other species (Betts et al., 2007; Hua et al., 2006; Schmolesky et al., 2000; Snowden and Kavanagh, 2006). For example, a study in aged humans shows a decrease in visual acuity, contrast sensitivity and motion sensitivity (Snowden and Kavanagh, 2006), and similar results were also found in other species such as monkey, cat as well as rodents (Hua et al., 2006; Schmolesky et al., 2000; Wang et al., 2006).

What is the mechanism for this ageing-related decrease in the orientation tuning? We observed the similar onset of both neuronal hyperactivity and decrease in orientation tuning and the negative correlation between the frequency of the spontaneous activity and OSI. Therefore, we suggest that a similar mechanism is responsible for both phenomena and that this mechanism is connected to an imbalance in the synaptic excitation and inhibition. This is supported by Ding et al.'s study, which documented a decline of intracortical inhibition in V1 of aged rats (Ding et al., 2017). In general, it is known that intracortical inhibition is a fundamental mechanism to modulate neuronal network activity in V1. Modelling studies suggest that intracortical inhibition sharpens neuronal responses by subtraction input. After subtraction, the weak inputs are removed, while the strong inputs are still remaining. On the other side, it divides all inputs to adjust the response gain from visual stimuli (Atallah et al., 2012; Carandini and Heeger, 1994; Lee et al., 2012; Monier et al., 2003; Wilson et al., 2012).

## 4.3 An impairment of visual response properties in mouse models of Alzheimer's disease

The results in this study represent one of the most complete analyses of the visual response properties in mouse models of AD. They document a significant impairment of visual processing in AD mice including (i) an overall increase in visual responsiveness, (ii) a profound decline of visual tuning properties and (iii) an impairment of the stimulus-induced suppression of spontaneous activity. Moreover, the degree of the impairment of visual tuning correlated with the level of neuronal activity. Interestingly, some (e.g. an overall increase in visual responsiveness, a decrease in direction selectivity) but not all of these alterations were also found in PS45 mice devoid of amyloid deposition and neuroinflammation (Fig. S4 in Lerdkrai et al, 2018), suggesting that these aspects of visual impairment are solely caused by a G384A mutation in a single allele of the presenilin 1 gene. We further show that an increased visual responsiveness in PS45 and AD mice is mainly caused by a dysfunction of the intracellular $Ca^{2+}$ stores because it can be normalized by CPA-mediated store depletion.

This study was conducted using a novel small molecule $Ca^{2+}$ indicator Cal-520, reported to yield $Ca^{2+}$ transients of larger amplitudes and higher signal-to-noise ratios compared to the commonly used Oregon Green BAPTA 1 (Tada et al., 2014). Despite these advantages of Cal-520, the fractions of visually responsive-neurons, measured in the current study, were similar to those observed by others (e.g. (Chen et al., 2013)) with Oregon Green BAPTA 1 or GCaMP6f.

By studying the same animal model of AD at a more advanced age, our data can directly be compared with the study conducted by Arthur Konnerth's group (Grienberger et al., 2012). Our data are consistent with the strong impairment of the orientation and a somewhat weaker impairment of the direction tuning found by the colleagues in 8-10 months old $APP_{SWE}/PS1_{G384A}$ mice. However, whereas the fractions of visually responsive-neurons were similar in 8-10 months old WT and AD mice (Grienberger et al., 2012), at the age studied here (10-12 months) a significantly larger fraction of cells in AD mice became visually responsive. Thus, our study is the first to reveal an AD-related increase in the number of visually responsive-neurons in the mammalian

primary visual cortex. This increase was largely independent of the precise nature of the visual stimuli but turned out to be somewhat stronger in AD compared to PS45 mice.

According to data presented here, the more advanced age of PS45 and AD mice is paralleled by an overall increase of neuronal hyperactivity in the visual cortex (compare **Figure 24** with Supplementary Figure S6 of (Grienberger et al., 2012)). Neuronal network hyperactivity is pronounced in AD mice and an increase in neuronal activity correlates significantly with a decrease in orientation selectivity and an increase in circular variance of visually responsive-neurons. Our study is also the first to describe the impairment of visual response properties in PS45 mice, as at younger age they were found to be asymptomatic (Grienberger et al., 2012). Moreover, in contrast to the data obtained by others (Grienberger et al., 2012), normal cells of AD mice at advanced age also had strongly impaired orientation and direction selectivity. Taken together, our data add one more stage to the description of the stage-specific decline of the visual response properties in this mouse model of AD. This stage is characterized by a strong increase in the fraction of hyperactive cells, an overall increase in visual responsiveness in AD compared to WT mice and an extension of the impairment of visual tuning properties onto an entire neuronal population (including normal and hyperactive cells) in AD mice.

Using another mouse model of AD ($APP_{SWE}/PS1_{L166P}$ mice) Liebscher et al. (Liebscher et al., 2016) could not observe any impairment of the visual response properties in 10-11 months old mice, despite the presence of substantial neuronal hyperactivity. The reason for this discrepancy remains unknown. One obvious difference is that their mice harbored another mutation in the presenilin gene, which might endow neurons with different functional properties (Zhang et al., 2010). Although experiments of Liebscher et al. were conducted in awake and ours as well as those of A. Konnerth's group (Grienberger et al., 2012) in anesthetized mice, this experimental difference is unlikely to account for the mentioned above discrepancy because the impairment of the visual processing was also present in awake $APP_{SWE}/PS1_{G384A}$ mice. Indeed, these mice were unable to discriminate drifting gratings of two different orientations separated by 22.5° (Grienberger et al., 2012). Moreover, Niell & Stryker

reported similar orientation selectivity and tuning width of mouse layer 2/3 neurons recorded in awake state and under anesthesia (Niell and Stryker, 2010).

### 4.4 Role of intracellular $Ca^{2+}$ stores for impairment of visual response properties in mouse models of Alzheimer's disease

Interestingly, some (e.g. an overall increase in visual responsiveness, a decrease in direction selectivity) but not all of the alterations that were detected in AD mice were also found in PS45 mice devoid of amyloid deposition and neuroinflammation (Lerdkrai et al., 2018), suggesting that these aspects of visual impairment are solely caused by a G384A mutation in a single allele of the presenilin 1 gene. This G384A mutation was shown to produce an overfilling of the intracellular $Ca^{2+}$ stores by abolishing presenilin-mediated $Ca^{2+}$ leak channel (Nelson et al., 2007). In addition, our *in vivo* study showed an effect of the G384A mutation on the neuronal hyperactivity via interfering with the presynaptic intracellular $Ca^{2+}$ stores, leading to an increase in glutamate release from the presynaptic terminals. Moreover, emptying intracellular $Ca^{2+}$ stores with CPA reversed neuronal hyperactivity in frontal/motor cortex (Lerdkrai et al., 2018). The present study shows that G384A mutation causes an increased visual responsiveness and that the increase in visual responsiveness can be normalized by CPA-mediated store depletion.

Because of the CPA sensitivity of this phenomenon and its presence in the heterozygous PS45 mice, we conclude that it is caused by the heightened $Ca^{2+}$ store-dependent release of an excitatory neurotransmitter (likely glutamate) from the presynaptic terminals. This observation adds a new facet to our knowledge about the neural network dysfunction in AD by showing that not only the spontaneous ongoing activity (Lerdkrai et al., 2018) but also the responses to sensory stimuli are potentiated by the AD-related mutation in the PS1 gene. As the modern human life is full of flickering photic stimuli (e.g. generated by TVs, computer games and electronic instruments with flickering displays) it is likely that in addition to causing exaggerated responses to visual stimuli, PS1-related increase in visual responsiveness is also

decreasing the threshold for induction of photically triggered synchronized neuronal discharges or even seizures (Martins da Silva and Leal, 2017).

### 4.5 Possible mechanisms underlying the impairment of the visual response properties

What are the possible mechanisms underlying the described above impairment of the visual response properties? The impairment of the direction selectivity in PS45 mice presenting with neuronal hyperactivity but not with amyloidosis and neuroinflammation, the lack of inhibition of spontaneous activity during the presentation of visual stimuli in AD mice, the overall increase in visual responsiveness in PS45 and AD compared to WT mice, and the correlation between the degree of visual impairment and that of neuronal hyperactivity on a single cell level all point to neuronal hyperactivity as the main cause of deterioration of visual response properties in AD mice. However, a significant reduction of neuronal hyperactivity by emptying the intracellular $Ca^{2+}$ stores improved some but not all aspects of AD-related visual dysfunction. The store depletion normalized the exaggerated visual responsiveness in PS45 and AD mice but the visual tuning properties still remained impaired.

If not stores-mediated neuronal hyperactivity, which mechanisms might contribute to the impairment of visual tuning properties in AD mice? The use of PS45 mice revealed dissociation between the impairment of the direction and the orientation selectivity. Although the overall degree of impairment of the direction selectivity in AD mice was smaller than that of the orientation selectivity, only the former was seen in PS45 mice. This data allows to exclude (i) accumulation of fibrillar amyloid β species, (ii) activation of astrocytes and microglia, (iii) neuronal hyperactivity as well as (iv) AD-related aggregation of tau protein in neurofibrillary tangles (Kuchibhotla et al., 2014) from the mechanisms underlying the impairment of the direction selectivity in AD mice. As for the impairment of orientation selectivity, the latter is more likely to be mediated via mechanisms triggered by amyloidosis or neuroinflammation. We suggest that one of such mechanisms might involve the dysfunction of parvalbumin-positive inhibitory

interneurons, initially observed in hAPP mice (Verret et al., 2012). Indeed, modulating spiking activity of $PV^+$ interneurons was recently shown to influence visual tuning properties of pyramidal neurons in the V1 (Atallah et al., 2012; Lee et al., 2012). Specifically, an acute optogenetically-induced excitation of $PV^+$ neurons caused a significant increase in the orientation and direction selectivity of layer 2/3 cells in awake as well as anesthetized state (Atallah et al., 2012; Lee et al., 2012), whereas a selective inhibition of $PV^+$ cells had an opposite effect (Atallah et al., 2012).

Another important result of our study is the discovery of the visual stimulation-induced inhibition of the ongoing spontaneous activity and of the impairment of this inhibition in a mouse model of AD. Together with the recent observation in the rat barrel cortex, where single or repetitive whisker deflections were also shown to inhibit the ongoing neuronal activity (Deneux and Grinvald, 2017), this finding identifies a general mechanism of interplay between the sensory-driven and spontaneous ongoing activities. This interplay appears to be bidirectional in nature, with ongoing spontaneous activity influencing the strength of sensory-evoked responses (Petersen et al., 2003) and vice versa, sensory-evoked responses influencing the ongoing spontaneous activity (this study and (Deneux and Grinvald, 2017)). In the barrel cortex sensory stimulation reduced firing of 57% of recorded neurons but increased firing of 7% of recorded cells (Deneux and Grinvald, 2017). We propose that the latter cells are parvalbumin- or somatostatin-expressing interneurons, inhibiting the surrounding pyramidal cells. In a mouse models of AD (hAPP and APP/PS1 mice), a PS1-mutation independent dysfunction of these inhibitory neurons (Schmid et al., 2016; Verret et al., 2012) is likely responsible for the lack of sensory-driven inhibition and the heightened ongoing activity during the presentation of the visual stimuli. This interfering ongoing activity is very likely to decrease decoding accuracy of V1 pyramidal neurons (Liebscher et al., 2016) causing AD-related deficits in visual discrimination in mice (Grienberger et al., 2012) and humans (Albers et al., 2015).

## 4.6 Clinical implications

As nowadays the life expectancy in the western societies is increasing, Alzheimer's disease is scaling up to one of the most serious worldwide health problems. Still, the current approved clinical drugs (e.g. memantine and cholinesterase blockers) provide only supportive or symptomatic treatment without ameliorating the pathogenesis of the disease (Schneider and Sano, 2009). In recent years, several newly proposed drugs, mainly targeting directly Aβ or β-secretase 1, are in the clinical trial phase. However, not all of them pass the clinical trials (Cummings et al., 2016; Sugino et al., 2015). For this reason, the better understanding of the cellular/molecular mechanisms underlying pathogenesis of AD are required.

The present study reveals a robust increase in neuronal hyperactivity in ageing and AD. It further shows that neuronal hyperactivity is associated with an impairment of neuronal responses to visual stimuli. Thus, our and several previous studies suggest that neuronal hyperactivity might be a candidate target for modifying both age- and AD-related functional impairments. Our previous study suggested that the intracellular $Ca^{2+}$ stores have an important role in controlling neuronal hyperactivity in AD (Lerdkrai et al., 2018). Current study further shows that CPA can significantly improve the pathological increase in visual responsiveness in mouse models of AD. Unfortunately, CPA can't improve an impairment of orientation and/or direction tuning properties in both mouse models of AD used in this study. This finding suggests that impairments of the visual tuning properties might be caused by an additional mechanism. Interestingly, CPA had no effect on age-related neuronal hyperactivity. Still, the strong correlation between neuronal hyperactivity and functional impairment of sensory properties found in this study asks for further study to search for an alternative strategy for reducing neuronal hyperactivity and improving the functional impairment in both ageing and Alzheimer's disease.

Apart from snew therapeutic candidate verification, our finding also suggests that neuronal hyperactivity might be a new potential marker for functional decline in both ageing and AD. Functional markers for the disease onset and progression are important for management of AD patients. Here, one of the big issues is how to timely document

the AD-related functional changes. Till now, the diagnosis criteria and standard monitoring of the disease uses clinical assessments together with brain imaging. However, this method has a low sensitivity. Alternative way of monitoring AD progression is an observing Aβ deposition. Using positron emission tomography of Pittsburg compound B allows visualizing the accumulation of Aβ in AD patients. However, the importance of Aβ deposition as an early marker of AD is still controversial, because the amount of Aβ deposits does not correlate with the level of functional impairment (Giannakopoulos et al., 2003; Huang and Mucke, 2012). Our results suggest that spontaneous neuronal activity or basal state neuronal activity might be a useful strategy for helping clinicians to monitor functional changes during the disease progression in AD patients.

# Conclusions

In summary, the data from this study is consistent with the view that the AD-related impairment of visual processing is caused by a complex change in the excitation/inhibition balance in the primary visual cortex. The latter comprises both a store dysfunction-mediated increase in neurotransmitter release from the glutamatergic axons, causing an overall increase in visual responsiveness, and an amyloid/neuroinflammation-mediated dysfunction of inhibitory interneurons, underlying the impairment of visual tuning and of the stimulus-induced suppression of spontaneous activity. Emptying intracellular $Ca^{2+}$ stores can improve an AD-related neuronal hyperresponsiveness to visual stimuli, but the AD-related impairment in orientation/direction tuning still remains impaired. It further shows that even in WT mice the aging-related neuronal hyperactivity in V1 develops simultaneously with an impairment of orientation tuning and therefore both phenomena are likely to be caused by a common mechanism, for example, a dysfunction of local inhibitory neurons. Interestingly, neuronal hyperactivity in V1 developed rather late compared to the frontal/motor cortex, suggesting a differential regional vulnerability to ageing.

# References


Albers, M. W., et al., 2015. At the interface of sensory and motor dysfunctions and Alzheimer's disease. Alzheimers Dement. 11, 70-98.

Association, A. s., 2018. 2018 Alzheimer's disease facts and figures. Alzheimer's & Dementia. 14, 367-429.

Atallah, B. V., et al., 2012. Parvalbumin-expressing interneurons linearly transform cortical responses to visual stimuli. Neuron. 73, 159-70.

Bakker, A., et al., 2012. Reduction of hippocampal hyperactivity improves cognition in amnestic mild cognitive impairment. Neuron. 74, 467-74.

Barresi, M., et al., 2012. Evaluation of olfactory dysfunction in neurodegenerative diseases. J Neurol Sci. 323, 16-24.

Berridge, M. J., et al., 1998. Calcium--a life and death signal. Nature. 395, 645-8.

Betts, L. R., et al., 2007. The effects of aging on orientation discrimination. Vision Res. 47, 1769-80.

Bezprozvanny, I., Mattson, M. P., 2008. Neuronal calcium mishandling and the pathogenesis of Alzheimer's disease. Trends Neurosci. 31, 454-63.

Bookheimer, S. Y., et al., 2000. Patterns of brain activation in people at risk for Alzheimer's disease. N Engl J Med. 343, 450-6.

Busche, M. A., et al., 2012. Critical role of soluble amyloid-beta for early hippocampal hyperactivity in a mouse model of Alzheimer's disease. Proc Natl Acad Sci U S A. 109, 8740-8745.

Busche, M. A., et al., 2008. Clusters of hyperactive neurons near amyloid plaques in a mouse model of Alzheimer's disease. Science. 321, 1686-9.

Cai, C., et al., 2006. The presenilin-2 loop peptide perturbs intracellular $Ca^{2+}$ homeostasis and accelerates apoptosis. J Biol Chem. 281, 16649-55.

Carandini, M., Heeger, D. J., 1994. Summation and division by neurons in primate visual cortex. Science. 264, 1333-6.

Cedazo-Minguez, A., et al., 2002. The presenilin 1 deltaE9 mutation gives enhanced basal phospholipase C activity and a resultant increase in intracellular calcium concentrations. J Biol Chem. 277, 36646-55.

Celone, K. A., et al., 2006. Alterations in memory networks in mild cognitive impairment and Alzheimer's disease: an independent component analysis. J Neurosci. 26, 10222-31.

Chakroborty, S., Stutzmann, G. E., 2014. Calcium channelopathies and Alzheimer's disease: insight into therapeutic success and failures. Eur J Pharmacol. 739, 83-95.

Chen, T. W., et al., 2013. Ultrasensitive fluorescent proteins for imaging neuronal activity. Nature. 499, 295-300.

Cheung, K. H., et al., 2008. Mechanism of $Ca^{2+}$ disruption in Alzheimer's disease by presenilin regulation of InsP3 receptor channel gating. Neuron. 58, 871-83.

Colonna, M., Wang, Y., 2016. TREM2 variants: new keys to decipher Alzheimer disease pathogenesis. Nat Rev Neurosci. 17, 201-7.

Corder, E. H., et al., 1993. Gene dose of apolipoprotein E type 4 allele and the risk of Alzheimer's disease in late onset families. Science. 261, 921-3.

Cronin-Golomb, A., et al., 1991. Visual dysfunction in Alzheimer's disease: relation to normal aging. Ann Neurol. 29, 41-52.

Cummings, J., et al., 2016. Drug development in Alzheimer's disease: the path to 2025. Alzheimers Res Ther. 8, 39.

Daulatzai, M. A., 2015. Olfactory dysfunction: its early temporal relationship and neural correlates in the pathogenesis of Alzheimer's disease. J Neural Transm (Vienna). 122, 1475-97.

Deneux, T., Grinvald, A., 2017. Milliseconds of Sensory Input Abruptly Modulate the Dynamics of Cortical States for Seconds. Cereb Cortex. 27, 4549-4563.

Devanand, D. P., et al., 2000. Olfactory deficits in patients with mild cognitive impairment predict Alzheimer's disease at follow-up. Am J Psychiatry. 157, 1399-405.

Dickerson, B. C., et al., 2005. Increased hippocampal activation in mild cognitive impairment compared to normal aging and AD. Neurology. 65, 404-11.

Ding, Y., et al., 2017. Changes in GABAergic markers accompany degradation of neuronal function in the primary visual cortex of senescent rats. Sci Rep. 7, 14897.

Dominguez-Gonzalez, M., et al., 2018. Regional vulnerability to lipoxidative damage and inflammation in normal human brain aging. Exp Gerontol. 111, 218-228.

Eichhoff, G., Garaschuk, O., 2011. Two-photon imaging of neural networks in a mouse model of Alzheimer's disease. Cold Spring Harb Protoc. 2011, 1206-16.

Flurkey K, et al., 2007. The Mouse in Aging Research. The Mouse in Biomedical Research, eds Fox JG, Davisson MT, Quimby FW, Barthold SW, Newcomer CE, & Smith AL (American College Laboratory Animal Medicine (Elsevier), Burlington, MA.). 637-672.

Garaschuk, O., et al., 2006. Targeted bulk-loading of fluorescent indicators for two-photon brain imaging in vivo. Nat Protoc. 1, 380-6.

Garaschuk, O., et al., 1997. Release and sequestration of calcium by ryanodine-sensitive stores in rat hippocampal neurones. J Physiol. 502 ( Pt 1), 13-30.

Gates, G. A., et al., 2008. Central auditory dysfunction in older persons with memory impairment or Alzheimer dementia. Arch Otolaryngol Head Neck Surg. 134, 771-7.

Gatz, M., et al., 2006. Role of genes and environments for explaining Alzheimer disease. Arch Gen Psychiatry. 63, 168-74.

Giannakopoulos, P., et al., 2003. Tangle and neuron numbers, but not amyloid load, predict cognitive status in Alzheimer's disease. Neurology. 60, 1495-500.

Goedert, M., Spillantini, M. G., 2006. A century of Alzheimer's disease. Science. 314, 777-81.

Gotz, J., et al., 2018. Rodent models for Alzheimer disease. Nat Rev Neurosci.

Goussakov, I., et al., 2010. NMDA-mediated $Ca^{2+}$ influx drives aberrant ryanodine receptor activation in dendrites of young Alzheimer's disease mice. J Neurosci. 30, 12128-37.

Green, K. N., et al., 2008. SERCA pump activity is physiologically regulated by presenilin and regulates amyloid beta production. J Cell Biol. 181, 1107-16.

Grienberger, C., et al., 2012. Staged decline of neuronal function in vivo in an animal model of Alzheimer's disease. Nat Commun. 3, 774.

Guerreiro, R., et al., 2013. TREM2 variants in Alzheimer's disease. N Engl J Med. 368, 117-27.

Guo, Q., et al., 1996. Alzheimer's PS-1 mutation perturbs calcium homeostasis and sensitizes PC12 cells to death induced by amyloid beta-peptide. Neuroreport. 8, 379-83.

Guo, Q., et al., 1997. Alzheimer's presenilin mutation sensitizes neural cells to apoptosis induced by trophic factor withdrawal and amyloid beta-peptide: involvement of calcium and oxyradicals. J Neurosci. 17, 4212-22.

Haass, C., 2004. Take five--BACE and the gamma-secretase quartet conduct Alzheimer's amyloid beta-peptide generation. EMBO J. 23, 483-8.

Haberman, R. P., et al., 2017a. Targeting Neural Hyperactivity as a Treatment to Stem Progression of Late-Onset Alzheimer's Disease. Neurotherapeutics. 14, 662-676.

Haberman, R. P., et al., 2017b. Heightened cortical excitability in aged rodents with memory impairment. Neurobiol Aging. 54, 144-151.

Hardy, J., 1997. Amyloid, the presenilins and Alzheimer's disease. Trends Neurosci. 20, 154-9.

Hermes, M., et al., 2010. Intracellular calcium signalling in Alzheimer's disease. J Cell Mol Med. 14, 30-41.

Holtzman, D. M., et al., 2011. Alzheimer's disease: the challenge of the second century. Sci Transl Med. 3, 77sr1.

Hua, T., et al., 2006. Functional degradation of visual cortical cells in old cats. Neurobiol Aging. 27, 155-62.

Huang, Y., Mucke, L., 2012. Alzheimer mechanisms and therapeutic strategies. Cell. 148, 1204-22.

Jarrett, J. T., Lansbury, P. T., Jr., 1993. Seeding "one-dimensional crystallization" of amyloid: a pathogenic mechanism in Alzheimer's disease and scrapie? Cell. 73, 1055-8.

Jonsson, T., et al., 2013. Variant of TREM2 associated with the risk of Alzheimer's disease. N Engl J Med. 368, 107-16.

Jucker, M., Walker, L. C., 2013. Self-propagation of pathogenic protein aggregates in neurodegenerative diseases. Nature. 501, 45-51.

Keskin, A. D., et al., 2017. BACE inhibition-dependent repair of Alzheimer's pathophysiology. Proc Natl Acad Sci U S A. 114, 8631-8636.

Kim, J., et al., 2009. The role of apolipoprotein E in Alzheimer's disease. Neuron. 63, 287-303.

Koh, M. T., et al., 2010. Treatment strategies targeting excess hippocampal activity benefit aged rats with cognitive impairment. Neuropsychopharmacology. 35, 1016-25.

Kuchibhotla, K. V., et al., 2014. Neurofibrillary tangle-bearing neurons are functionally integrated in cortical circuits in vivo. Proc Natl Acad Sci U S A. 111, 510-4.

Lee, S. H., et al., 2012. Activation of specific interneurons improves V1 feature selectivity and visual perception. Nature. 488, 379-83.

Lerdkrai, C., et al., 2018. Intracellular $Ca^{2+}$ stores control in vivo neuronal hyperactivity in a mouse model of Alzheimer's disease. Proc Natl Acad Sci U S A. 115, E1279-E1288.

Liebscher, S., et al., 2016. Selective Persistence of Sensorimotor Mismatch Signals in Visual Cortex of Behaving Alzheimer's Disease Mice. Curr Biol. 26, 956-64.

Maier, F. C., et al., 2014. Longitudinal PET-MRI reveals beta-amyloid deposition and rCBF dynamics and connects vascular amyloidosis to quantitative loss of perfusion. Nat Med. 20, 1485-92.

Martins da Silva, A., Leal, B., 2017. Photosensitivity and epilepsy: Current concepts and perspectives-A narrative review. Seizure. 50, 209-218.

Mattson, M. P., 2010. ER calcium and Alzheimer's disease: in a state of flux. Sci Signal. 3, pe10.

Mattson, M. P., Magnus, T., 2006. Ageing and neuronal vulnerability. Nat Rev Neurosci. 7, 278-94.

Mesholam, R. I., et al., 1998. Olfaction in neurodegenerative disease: a meta-analysis of olfactory functioning in Alzheimer's and Parkinson's diseases. Arch Neurol. 55, 84-90.

Minkeviciene, R., et al., 2009. Amyloid beta-Induced Neuronal Hyperexcitability Triggers Progressive Epilepsy. Journal of Neuroscience. 29, 3453-3462.

Monier, C., et al., 2003. Orientation and direction selectivity of synaptic inputs in visual cortical neurons: a diversity of combinations produces spike tuning. Neuron. 37, 663-80.

Naudi, A., et al., 2017. Region-specific vulnerability to lipid peroxidation and evidence of neuronal mechanisms for polyunsaturated fatty acid biosynthesis in the healthy adult human central nervous system. Biochim Biophys Acta Mol Cell Biol Lipids. 1862, 485-495.

Nelson, O., et al., 2007. Familial Alzheimer disease-linked mutations specifically disrupt $Ca^{2+}$ leak function of presenilin 1. J Clin Invest. 117, 1230-9.

Niell, C. M., Stryker, M. P., 2008. Highly selective receptive fields in mouse visual cortex. J Neurosci. 28, 7520-36.

Niell, C. M., Stryker, M. P., 2010. Modulation of visual responses by behavioral state in mouse visual cortex. Neuron. 65, 472-9.

O'Brien, C., 1996. Auguste D. and Alzheimer's disease. Science. 273, 28.

Palop, J. J., et al., 2006. A network dysfunction perspective on neurodegenerative diseases. Nature. 443, 768-73.

Palop, J. J., et al., 2007. Aberrant excitatory neuronal activity and compensatory remodeling of inhibitory hippocampal circuits in mouse models of Alzheimer's disease. Neuron. 55, 697-711.

Palop, J. J., Mucke, L., 2016. Network abnormalities and interneuron dysfunction in Alzheimer disease. Nat Rev Neurosci. 17, 777-792.

Petersen, C. C., et al., 2003. Interaction of sensory responses with spontaneous depolarization in layer 2/3 barrel cortex. Proc Natl Acad Sci U S A. 100, 13638-43.

Risacher, S. L., et al., 2013. Visual contrast sensitivity in Alzheimer's disease, mild cognitive impairment, and older adults with cognitive complaints. Neurobiol Aging. 34, 1133-44.

Rizzo, M., et al., 2000. Vision and cognition in Alzheimer's disease. Neuropsychologia. 38, 1157-69.

Schmid, L. C., et al., 2016. Dysfunction of Somatostatin-Positive Interneurons Associated with Memory Deficits in an Alzheimer's Disease Model. Neuron. 92, 114-125.

Schmolesky, M. T., et al., 2000. Degradation of stimulus selectivity of visual cortical cells in senescent rhesus monkeys. Nat Neurosci. 3, 384-90.

Schneider, L. S., Sano, M., 2009. Current Alzheimer's disease clinical trials: methods and placebo outcomes. Alzheimers Dement. 5, 388-97.

Shen, J., Kelleher, R. J., 3rd, 2007. The presenilin hypothesis of Alzheimer's disease: evidence for a loss-of-function pathogenic mechanism. Proc Natl Acad Sci U S A. 104, 403-9.

Simkin, D., et al., 2015. Aging-Related Hyperexcitability in CA3 Pyramidal Neurons Is Mediated by Enhanced A-Type $K^+$ Channel Function and Expression. J Neurosci. 35, 13206-18.

Siskova, Z., et al., 2014. Dendritic structural degeneration is functionally linked to cellular hyperexcitability in a mouse model of Alzheimer's disease. Neuron. 84, 1023-33.

Snowden, R. J., Kavanagh, E., 2006. Motion perception in the ageing visual system: minimum motion, motion coherence, and speed discrimination thresholds. Perception. 35, 9-24.

Spat, A., et al., 2008. High- and low-calcium-dependent mechanisms of mitochondrial calcium signalling. Cell Calcium. 44, 51-63.

Steiner, H., Haass, C., 2000. Intramembrane proteolysis by presenilins. Nat Rev Mol Cell Biol. 1, 217-24.

Stieren, E., et al., 2010. FAD mutations in amyloid precursor protein do not directly perturb intracellular calcium homeostasis. PLoS One. 5, e11992.

Stosiek, C., et al., 2003. In vivo two-photon calcium imaging of neuronal networks. Proc Natl Acad Sci U S A. 100, 7319-24.

Stothart, G., et al., 2015. Early visual evoked potentials and mismatch negativity in Alzheimer's disease and mild cognitive impairment. J Alzheimers Dis. 44, 397-408.

Stutzmann, G. E., et al., 2006. Enhanced ryanodine receptor recruitment contributes to $Ca^{2+}$ disruptions in young, adult, and aged Alzheimer's disease mice. J Neurosci. 26, 5180-9.

Sugino, H., et al., 2015. Global Trends in Alzheimer Disease Clinical Development: Increasing the Probability of Success. Clin Ther. 37, 1632-42.

Tada, M., et al., 2014. A highly sensitive fluorescent indicator dye for calcium imaging of neural activity in vitro and in vivo. Eur J Neurosci. 39, 1720-8.

Tandon, A., Fraser, P., 2002. The presenilins. Genome Biol. 3, reviews3014.

Tu, H., et al., 2006. Presenilins form ER $Ca^{2+}$ leak channels, a function disrupted by familial Alzheimer's disease-linked mutations. Cell. 126, 981-93.

Verret, L., et al., 2012. Inhibitory interneuron deficit links altered network activity and cognitive dysfunction in Alzheimer model. Cell. 149, 708-21.

Wang, H., et al., 2006. Functional degradation of visual cortical cells in aged rats. Brain Res. 1122, 93-8.

Wilson, N. R., et al., 2012. Division and subtraction by distinct cortical inhibitory networks in vivo. Nature. 488, 343-8.

Yassa, M. A., et al., 2011. Pattern separation deficits associated with increased hippocampal CA3 and dentate gyrus activity in nondemented older adults. Hippocampus. 21, 968-79.

Zeger, S. L., Liang, K. Y., 1986. Longitudinal data analysis for discrete and continuous outcomes. Biometrics. 42, 121-30.

Zhang, C., et al., 2009. Presenilins are essential for regulating neurotransmitter release. Nature. 460, 632-6.

Zhang, H., et al., 2010. Role of presenilins in neuronal calcium homeostasis. J Neurosci. 30, 8566-80.

Zou, Y. M., et al., 2016. Olfactory dysfunction in Alzheimer's disease. Neuropsychiatr Dis Treat. 12, 869-75.

# Acknowledgements

First of all, I would like to express my sincere thanks for Professor Dr. Olga Garaschuk, who supported me from the beginning of this work. She always teaches me how to improve my critical thinking which is not only helpful for my PhD study but also very helpful for my further scientific career. I have to thank Dr. Bianca Brawek for her kindly encouragement and suggestion, Dr. Chommanad Lerdkrai who helped and taught me the experiment procedures and Dr. Yury Kovalchuk who suggested and helped me with the experimental setup. I would like to thank the other members of my committee, Professor Manuela Neumann and Professor Laura Busse for their suggestions. I would like to thank Karl Schöntag, Andrea Weible and Elizabeta Zirdum for their technical support. In addition, I would like to thank every single person of Institute of Physiology who supported and helped me for this work. At the end, I would like to dedicate this work to my parents and my brother who always trust and encourage me to pursue my dream of becoming a scientist.